Algal lipid distributions and hydrogen isotope ratios reflect phytoplankton community dynamics

Antonia Klatt[1], Cindy De Jonge[2], Daniel B. Nelson[3], Marta Reyes[4], Carsten J. Schubert[5,6], Nathalie Dubois[2,7] & S. Nemiah Ladd[1]

[1]University of Basel, Department of Environmental Sciences, Organic Geochemistry, Basel, Switzerland

[2]ETH Zurich, Department of Earth Sciences, Zurich, Switzerland

[3]University of Basel, Department of Environmental Sciences, Botany, Basel, Switzerland

[4]Swiss Federal Institute of Aquatic Science and Technology (Eawag), Department Aquatic Ecology, Dübendorf, Switzerland

[5]Swiss Federal Institute of Aquatic Science and Technology (Eawag), Department Surface Waters – Research and Management, Kastanienbaum, Switzerland

[6]ETH Zurich, Department of Environmental System Science, Zurich, Switzerland

[7]Swiss Federal Institute of Aquatic Science and Technology (Eawag), Department Surface Waters – Research and Management, Dübendorf, Switzerland

Email addresses: Antonia.klatt@unibas.ch, cindy.dejonge@erdw.ethz.ch, daniel.nelson@unibas.ch, Marta.Reyes@eawag.ch, Carsten.Schubert@eawag.ch, Nathalie.Dubois@eawag.ch, n.ladd@unibas.ch

This is a non-peer-reviewed preprint submitted to EarthArXiv. This preprint has been submitted for peer review at *Geochimica et Cosmochimica Acta*. This version of the manuscript has been modified to incorporate one round of feedback from three peer reviewers.

Abstract

Reconstructions of past changes in algal community composition provide important context for future alterations in biogeochemical cycling. However, many existing phytoplankton proxies are indicative of individual algal groups and are not fully representative of the whole community. Here, we evaluated hydrogen isotope ratios of algal lipids (δ^2H_{Lipid}) as a potential proxy for phytoplankton community composition. We sampled the water column of Rotsee, a small eutrophic lake in Switzerland, every second week from January 2019 to February 2020 and analyzed distributions and the relative offsets between δ^2H_{Lipid} values ($\delta^2H_{Lipid1/Lipid2}$) from short-chain fatty acids, phytosterols and phytol. Comparing these data with phytoplankton cell counts, we found $\delta^2H_{C16:0\ Acid/Sterol}$ and $\delta^2H_{Sterol/Phytol}$ values reflect shifts in the eukaryotic algal community. To assess whether the selected phytoplankton groups were the main sources of the selected lipids, we further modeled algal $\delta^2H_{Lipid1/Lipid2}$ values based on $\delta^2H_{C16:0\ Acid}$, δ^2H_{Sterol} and δ^2H_{Phytol} values from batch cultures of individual algal groups and their biovolume in Rotsee and evaluated the role of heterotrophy on $\delta^2H_{Lipid1/Lipid2}$ values using a model incorporating $\delta^2H_{C16:0\ Acid}$ and δ^2H_{Sterol} values from microzooplankton. Annually-integrated and amount-weighted $\delta^2H_{Lipid1/Lipid2}$ values measured in Rotsee were within 2 to 20 ‰ of the mean of modeled algal $\delta^2H_{Lipid1/Lipid2}$ values, demonstrating a strong link with the phytoplankton community composition, while $\delta^2H_{Lipid1/Lipid2}$ values including microzooplankton lipids had a larger offset. Additionally, cyanobacterial biovolume was positively correlated with the ratio of phytol and phytosterols (phytol:sterol ratio) as well as the ratio of unsaturated C18 and C16:0 fatty acids (C18:C16 ratio). Our results support the application of sedimentary $\delta^2H_{Lipid1/Lipid2}$ values in eutrophic lakes as a proxy for past phytoplankton community assemblages. Moreover, the calculation of sedimentary phytol:sterol and C18:C16 ratios provides an additional proxy for reconstructing cyanobacterial blooms.

Key words: Algae, lipid biomarkers, hydrogen isotopes, eutrophic lakes

1. Introduction

In recent decades, temperate lakes have been increasingly impacted by anthropogenic eutrophication and climate change, leading to changes in phytoplankton communities (e.g., Shimoda *et al.*, 2011; McGowan *et al.*, 2012; Callisto *et al.*, 2014; Huisman *et al.*, 2018; Lin *et al.,* 2021). The composition of lacustrine phytoplankton communities greatly impacts biogeochemical cycling of carbon, nitrogen, and phosphorus (Ptacnik *et al.,* 2008; Litchman *et al.*, 2015; Naselli-Flores & Padisák, 2023), as well as higher trophic levels in aquatic food webs (e.g., Wacker & Martin-Creuzberg 2012). To predict future changes in phytoplankton community composition, modeling approaches incorporate results from culturing studies and observations of algal responses to biotic and abiotic factors (e.g., Arhonditsis *et al.,* 2006, Acevedo-Trejos *et al.,* 2015; Henson *et al.,* 2021; Mattern *et al.*, 2022; Liu *et al.,* 2023). However, long-term impacts of climate and environmental changes are difficult to replicate in algal cultures and short-term community feedbacks. Therefore, reconstructions of past phytoplankton community changes over longer timescales (decades, centuries, millennia) offer important insights for modeling future dynamics (e.g., Shen et al., 2018; Cvetkoska *et al.,* 2021).

Diverse proxies for estimating past phytoplankton community compositions exist, each associated with its own limitation and biases. For instance, paleolimnologists often quantify the abundance of dinoflagellate cysts or diatom silicate frustules (e.g., Dale & Fjellså 1994; Lotter 1998; Hinder *et al.,* 2021; Cvetkoska *et al.,* 2021), but only limited taxa produce fossil remains, so these are not representative of the whole community. Other reconstructions are based on pigments (e.g., Leavitt 1993; Reuss *et al.*, 2005), or sedimentary ancient DNA (*sed*aDNA) (Capo *et al.,* 2022), two compound classes that can be impacted by degradation and associated preferential diagenesis (Reuss *et al.,* 2005; Capo *et al.,* 2015; Nwosu *et al.,* 2023; Thorpe *et al.,* 2024)

Due to their good preservation over geological times, algal membrane lipids in sediments and rocks have been used to trace past phytoplankton abundance (e.g., Schubert *et al.,* 1998; Naeher *et al.,* 2012; Brocks *et al.,* 2017; Summons *et al.,* 2022; Zeman-Kuhnert *et*

*al.,*2023). For example, eukaryotic and bacterial membranes contain saturated and unsaturated short-chain fatty acids, such as C16:0, C16:1, C18:0, C18:1 or C18:3 (Killops & Killops 2004; Rustan & Drevon 2005; Li *et al*., 2010; Taipale *et al*., 2013). Additionally, eukaryotes modify membrane fluidity and permeability by the incorporation of sterols (Volkman 2003; Dufourc 2008; Desmond & Gribaldo 2009). Typical sterols of photoautotrophic eukaryotes, i.e., plants and microalgae, are brassicasterol (24-methylcholesta-5,22-dien-3β-ol), stigmasterol (24-ethylcholesta-5,22-dien-3β-ol) and sitosterol (24-ethylcholest-5-en-3β-ol) (Killops & Killops 2004; Piironen *et al.,* 2000; Taipale *et al.,* 2016; Peltomaa *et al.,* 2023). Despite bacterial gene homologues potentially encoding enzymes involved in sterol synthesis (Wei *et al.,* 2016), cyanobacteria have been found to generally lack any sterols (e.g., Volkman 2003; Martin-Creuzburg *et al.,* 2008; Taipale *et al.,* 2016; Peltomaa *et al.,* 2023). In addition to membrane lipids, phytol ((2E,7R,11R)-3,7,11,15-Tetramethyl-2-hexadecen-1-ol), the ester-linked side-chain of chlorophyll, is preserved in sediment and interpreted as lipid biomarker for all phototrophs (e.g., Rontani & Volkman 2003; Killops & Killops 2004; Witkowski *et al.,* 2020). Some compounds have been used as proxies for specific phytoplankton groups (e.g., Mouradian *et al.,* 2007; Yuan *et al.,* 2020), but many lipids are not as source-specific as initially thought (e.g., Rampen *et al.,* 2010). Rather than focusing on source-specific biomarkers, a more holistic analysis of lipid distributions might highlight shifts in the phytoplankton community with a greater robustness.

In addition to the variability in lipid biomarkers, phytoplankton community composition might be reflected in the hydrogen isotope ratios of algal lipids, i.e., δ^2H_{Lipid} values ($\delta^2H = (^2H/^1H)_{sample}/(^2H/^1H)_{VSMOW} - 1$). Initially considered as a proxy for δ^2H values of past lake water (e.g., Sauer *et al.,* 2001; Huang *et al.,* 2004), algal δ^2H_{Lipid} values have been found to be impacted by algal growth rate, salinity, temperature and CO_2 limitation (e.g., Z. Zhang *et al.,* 2009; Sachs & Schwab 2011; Nelson & Sachs 2014; Sachs & Kawka 2015; Torres-Romero *et al.,* 2024) and there is increasing evidence of a strong ecological signal recorded in algal δ^2H_{Lipid} values. Due species-specific variability in hydrogen isotope fractionation between lipids and water (i.e., $\alpha^2_{Lipid/Water} = (^2H/^1H_{Lipid})/(^2H/^1H_{Water})$), δ^2H_{Lipid} values vary

significantly among different algal groups grown under identical conditions in laboratory cultures (Schouten *et al.,* 2006; Zhang & Sachs 2007; M'Boule *et al.,* 2014; Heinzelmann *et al.,* 2015a; Ladd *et al.,* 2025; Pilecky et al., 2024).

Yet, changes in δ^2H values of lake water might still be recorded in algal lipids as the hydrogen for lipid synthesis originates from source water (e.g., Sachse *et al.*, 2012). The potential isotopic signal from lake water on δ^2H_{Lipid} values is excluded by using relative offsets between δ^2H_{Lipid} values (i.e., $\delta^2H_{Lipid1/Lipid2} = (\delta^2H_{Lipid1}+1)/(\delta^2H_{Lipid2}+1) - 1$). Although the magnitude of change in δ^2H_{Lipid} values resulting from changes in δ^2H_{water} differs among algal groups, $\delta^2H_{Lipid1/Lipid2}$ values are stable since the different phytoplankton groups use the same source water for lipid synthesis. Culturing and mesocosm experiments have shown that $\delta^2H_{Lipid1/Lipid2}$ values strongly differ among different phytoplankton groups (Ladd *et al.,* 2025; Pilecky *et al*., 2024). For example, $\delta^2H_{C16:0\ Acid/Phytol}$ values for green algae and cyanobacteria were up to 150 ‰ higher than for diatoms, cryptomonads and dinoflagellates, while $\delta^2H_{C16:0\ Acid/Sterol}$ values for diatoms were > 250 ‰ lower than for green algae. This ecological range in algal δ^2H_{Lipid} values exceeds the difference between δ^2H values of precipitation in the subtropics and boreal zones (e.g., Darling *et al*., 2006), as well as changes in isotopic precipitation signatures during glacial/interglacial cycles (e.g., Vimeux *et al*., 1999; Osman *et al.,* 2021).

In this study, we evaluated $\delta^2H_{Lipid1/Lipid2}$ values as a proxy for phytoplankton community composition in a natural lacustrine system and sought to improve the reconstruction of algal communities based on lipid biomarker distributions. For this aim, samples were taken from the water column of Rotsee, a small eutrophic lake in central Switzerland, every second week from January 2019 to February 2020. Cell counts of phytoplankton and microzooplankton were conducted and lipid abundances as well as compound-specific δ^2H_{Lipid} values of short-chain fatty acids, sterols and phytol were measured. We compared $\delta^2H_{Lipid1/Lipid2}$ values and lipid distributions to phytoplankton biovolume to assess how lipid-based indicators captured algal community shifts throughout the year. Specifically, we

analyzed whether cyanobacterial and green algal blooms are reflected by $\delta^2H_{C16:0\ Acid/Phytol}$ values and if changes in the eukaryotic algal community composition can be inferred from $\delta^2H_{C16:0\ Acid/Sterol}$ and $\delta^2H_{Sterol/Phytol}$ values. Furthermore, we modeled $\delta^2H_{Lipid1/Lipid2}$ values incorporating biovolume-weighted δ^2H_{Lipid} values from microzooplankton to investigate potential heterotrophic signatures in $\delta^2H_{Lipid1/Lipid2}$ values.

2. Methods

2.1 Study site and sample collection

Rotsee is a small (0.47 km^2 surface area), monomictic and eutrophic lake in central Switzerland (47°04′11″N 8°18′51″E) (Fig. S1) at 419 m asl (Bloesch 1974; Lotter 1989). The maximal depth is 16 m with a total volume of $4.3x10^6$ m^3 (Bloesch 1974). During the one-year sampling period, depth profiles of turbidity, conductivity, temperature, pH and dissolved oxygen were measured by different multi-parameter CTD probes (75M, Sea and Sun Marine Tech, Trappenkamp, Germany; WTW, Weilheim, Germany). Temperatures at specific sampling depths were estimated by the mean of temperatures from 0.5 m above to 0.5 m below the respective depth.

Sampling occurred every second week near the lake's center (Fig. S1) from January 2019 to February 2020 on mostly sunny mornings. Samples were taken at 1 m depth and at the depth of chlorophyll maximum, as determined based on the turbidity maximum on the respective sampling date measured by the multi-parameter CTD probe. Chlorophyll maximum depths ranged from 5 m to 14 m. If no turbidity maximum was present, samples were collected at 4 m depth. Lake water was filtered through a pre-combusted (6 hours at 450 °C) 142 mm Whatman® GF/F filter (pore size 0.7 µm) with a WTS-LV Large Volume Pump (12-40 l; McLane, MA, USA). Filters were wrapped in pre-combusted aluminum foil, kept on ice during transport, and stored at -20 °C until further analysis. Water samples for phytoplankton, water isotope measurements and nutrient analyses were collected with a

Niskin Water Sampler at the same depths (5 l; Hydro-Bios, Altenholz, Germany). For phytoplankton samples, 40 ml water were directly fixed with 5 ml lugol solution (5% iodide, 10% potassium iodide) and stored in the dark at 4°C until identification, which occurred within a few weeks. For water isotope samples, 2 ml water were filtered through a 25 mm syringe filter with a 0.45 μm polyethersulfone membrane into 2 ml vials and stored at 4 °C prior to analysis. Samples for nutrient analysis were filtered through cellulose acetate (pore size 0.45 μm) and stored in opaque bottles at 4 °C prior to analysis.

2.2 Nutrient concentrations

Total phosphorus concentrations were measured according to Vogler (1965) with modifications. Following chemical digestion with potassium peroxodisulfate at 121 °C, ortho-phosphate concentrations were determined after the reaction to a phosphorus-molybdenum-blue-complex with a spectrophotometer (Cary 60, Agilent, Santa Clara, CA, USA). Total nitrogen concentrations were measured by chemiluminescence with a Total Organic Carbon Analyzer with Total Nitrogen Unit (TOC-L CSH, Shimadzu, Nakagyo-ku, Kyōto, Japan).

2.3 Microscopy and biovolume calculation

A sub-sample (3 ml or 10 ml depending on density) was sedimented and counted in an Utermöhl-chamber (Hydro-Bios) (von Utermöhl, 1931). Phytoplankton cells were identified and counted manually with an inverted microscope (Zeiss Axiovert 135, Carl Zeiss, Oberkochen, Germany) using a 20x and 40x objective lens with 10x eyepiece and a 1.6x optovar lens (320x and 640x total magnification; 40 fields in each magnification). Phytoplankton samples were analyzed microscopically, since sequencing environmental DNA would not provide the morphological information to calculate phytoplankton biovolume, which is relevant for assessing the contribution of each algal group to the lipid pool. Identifications were performed to the greatest possible taxonomic level (generally genus or

species). Since rare species might not be present in the counted fields, their abundance was additionally analyzed and estimated in a whole transect at a magnification of 320x to gain a better representation of the whole phytoplankton community. Cell densities were normalized to an appropriate volume (cells/l) and the biovolume of different phytoplankton groups was calculated by multiplying the cell densities of the corresponding species by their mean per-cell biovolume. Biovolume values were based on biovolume measurements from individual phytoplankton cells from Greifensee according to standard protocols (Narwani *et al.,* 2019).

2.4 Lipid extraction and quantification

All glassware and utensils used for lipid extraction and purification were pre-combusted or solvent-cleaned with dichloromethane (DCM):methanol (MeOH) (9:1 (v/v)).

Total lipid extracts (TLEs) for fatty acid and phytol analyses were extracted from half of a freeze-dried filter sample in a SOLVpro microwave reaction system (Anton Paar, Graz, Austria) in 30 ml 9:1 DCM:MeOH for 5 min at 70 °C according to Ladd *et al.* (2017). Prior to extractions, 10.04 µg 1-nonadecanol (*n*-C19-alkanol), 10.8 µg 5α-androstane, 10.3 µg 3-eicosanone, and 9.6 µg nonadecanoic acid (*n*-C19-acid) were added as internal standards to each sample. TLEs for sterol analyses were extracted from the other half of the dry filter sample with an accelerated solvent extraction system (ASE) (Dionex™ ASE™ 350, Thermo Fisher Scientific, Waltham, MA, USA) according to Hirave *et al.* (2021). Briefly, samples were loaded between glass fiber filters in 34 ml stainless steel vessels and extra volume was filled up with Ottawa sand (Thermo Fisher Scientific). TLEs were extracted in 9:1 DCM:MeOH at 100 °C with a pressure of 100 bar on each cell and three 5-min static phases. Prior to ASE extractions, an internal standard containing 47.2 µg heneicosanol (*n*-C21-alkanol), 68.2 µg hexatriacontane (*n*-C36-alkane), 46.8 µg nonadecanoic acid (*n*-C19-acid) and 47 µg 2-octadecanone was added to each sample.

Dry TLEs were saponified with ~ 3 ml 1 N potassium hydroxide (KOH) in MeOH for 3-16 hours at 70 °C with varying saponification times having no expected impact on saponification

efficiency. After saponification, 2 ml of MilliQ water was added to each sample and the neutral fraction was extracted using multiple heptane rinses. The aqueous phase containing the acid fraction was acidified to pH < 2 and the protonated acid fraction was extracted using multiple heptane rinses.

A subset of neutral fractions was further purified by silica gel column chromatography according to Ladd *et al*. (2017) to obtain the alcohol fraction. Samples were dissolved in hexane and transferred onto a 500 mg/6ml Isolute silica gel column (Biotage, Uppsala, Sweden) and *n*-alkanes were eluted with 4 ml hexane, aldehydes and ketones with 1:1 hexane:DCM, alcohols in 9:1 DCM:MeOH and polar compounds in MeOH. As no compounds were present in the other purified fractions, alcohols were subsequently analyzed in unpurified neutral fractions. The neutral or alcohol fraction was acetylated with 200 µl pyridine and 25 µl acetic anhydride for 30 min at 70 °C. The δ^2H values of the added acetyl group were estimated by mass balance calculation after the acetylation of *n*-C_{21}-alkanol or sucrose with a known δ^2H value. Additionally, δ^2H values of acetic anhydride were further measured on a high-temperature conversion/elemental analyzer (TC/EA) (Thermo Fisher Scientific) coupled to a Delta V plus isotope ratio mass spectrometer (IRMS) (Thermo Fisher Scientific) *via* a ConFlo IV interface (Thermo Fisher Scientific) following Newberry *et al.* (2017).

Acid fractions were methylated with 4 ml 95:5 MeOH:hydrochloric acid (HCl) at 70 °C for ~ 16 hours. Methylated samples were mixed with 4 ml of 0.1 M potassium chloride (KCl) in MilliQ water and fatty acid methyl-esters (FAMEs) were extracted by serial heptane rinses. The δ^2H value of the added methyl group was determined by mass balance calculation after the methylation of phthalic acid of a known δ^2H value (Arndt Schimmelmann, Indiana University).

Acetylated alcohols (phytol and sterols) and FAMEs were quantified by gas chromatography–flame ionization detection (GC-FID) with an InertCap 5MS/NP column (30 m x 0.25 mm x 0.25 µm) (GL Sciences, Japan) according to Ladd *et al.* (2017) (alcohols) or a Trace™ 1310 gas chromatograph (Thermo Fisher Scientific) with a Rtx-5MS column (30 m x

0.25 mm x 0.25 µm) (Restek, Bad Homburg vor der Höhe, Germany) according to Baan *et al.* (2023) (FAMEs). Sterols and phytol were initially identified by analyzing the mass spectra of a subset of samples by gas chromatography-mass spectrometry (GC-MS) according to Ladd *et al.* (2017) under the same conditions as for GC-FID analyses. Further identification of sterols and phytol occurred based on their elution order and relative peak areas. FAMEs were identified by comparing retention times to an external standard (Sulpelco® 37-component FAME Mix, reference no. 47885U) (Merck KGaA, Darmstadt, Germany).

2.5 Lipid δ^2H measurements

Lipid δ^2H values were measured by gas chromatography-isotope ratio mass spectrometry (GC-IRMS) on a Trace GC Ultra (Thermo Fisher Scientific) coupled to a Delta V plus IRMS (Thermo Fisher Scientific) with a ConFlo IV interface (Thermo Fisher Scientific). Samples were injected with an AS TriPlus autosampler (Thermo Fisher Scientific) to a split/splitless inlet operated in splitless mode at 280 °C. FAMEs were measured on a Rtx-2330 column (30 m x 0.25 mm x 0.20 µm) (Restek), which was heated from 60 to 130 °C at 15 °C/min, from 130 to 265 °C at 8 °C/min and held at 265 °C for 5 min. Alcohols were measured on a Rtx-5MS column (30m x 0.25mm x 0.25µm) (Restek) which was heated from 60 to 120 °C at 15 °C/min, from 120 to 325 °C at 5 °C/min and held at 325 °C for 10 min. Column effluent was pyrolyzed at 1420 °C.

Measured hydrogen isotope values from the Thermo Isodat 3.0 software were converted to the Vienna Standard Mean Ocean Water (VSMOW) scale with regression models between measured and externally provided δ^2H values for reference standard compounds, which were analyzed at the beginning and the end of each sequence and between at most ten sample injections. Normalization included an initial linear regression between measured and known δ^2H values and a second multiple linear regression to correct for drift and isotopic effects related to peak size and retention time. Reference standards included *n*-alkane Mix

A7 and FAME Mix F8-3 (Arndt Schimmelmann, Indiana University), and C20:0 FAME USGS71 (United States Geological Survey).

δ^2H_{Sterol} values were further corrected for biases related to peak dimensions due to variable size effects between sterols and the aliphatic standards. Cholesterol acetate and stigmasterol acetate stock compounds (Merck) were measured at different concentrations ranging from 50 ng to 2 µg to determine the threshold peak area for stable δ^2H values, which was ~ 40 Vs (Fig. S3A). δ^2H values of the same stock compounds were separately calibrated through bulk sample measurements done on a TC/EA IRMS (Thermo Fisher Scientific) according to Holloway-Phillips *et al.* (2023) without dual water equilibration (cholesterol acetate) or as the average of δ^2H values at appropriate peak areas (stigmasterol acetate). The resulting relationship between peak area and the relative isotopic offset between measured and calibrated δ^2H values ($\delta^2H_{measured/calibrated}$) (Fig. S3B) was used to correct δ^2H_{sterol} values based on their individual peak areas.

Quality control standards (*n*-C29,32 alkanes (Stable Isotope Ecology Laboratory, University of Basel); C20:0 FAME (USGS70, United States Geological Survey); Supelco® C8-C24 FAME Mix (reference no CRM18918, Merck)) were measured throughout each sequence and scale normalized to VSMOW in the same way as the samples. Of these, the *n*-C32 alkane and the C20:0 FAME were purchased isotope reference materials with known δ^2H values, while δ^2H values of the remaining compounds have been routinely measured to track long term measurement precision. The average standard deviation (SD) for all quality control compounds together was 2 ‰, with an average offset of 0.4 ‰ from their known value (n = 467). The H_3^+ factor was determined in the beginning of each sequence and averaged 2.8 +/- 0.2 ppm nA^{-1}. Sample δ^2H values were further corrected for hydrogen added during derivatization based on isotopic mass balance. Errors were estimated from replicate measurements and the uncertainties associated with the added hydrogen.

2.6 Water δ^2H measurements

Water δ^2H values were measured on a TC/EA IRMS (Thermo Fisher Scientific) according to Newberry *et al.* (2017). Two water standards with known δ^2H values were injected at the beginning and the end of each sequence and after every 14 sample injections. Values were normalized to the VSMOW scale using measured and known δ^2H values of laboratory working standards and included corrections for time-based drift and memory effects. As a quality control, another water standard was injected at the beginning and the end of each sequence and after every 14 sample injections and corrected in the same way as the samples. The SD of the standard averaged 0.26 ‰ and the average offset from the known value was 0.05 ‰.

2.7 Calculations & statistics

Statistical analyses and modeling of $\delta^2H_{Lipid1/Lipid2}$ values were carried out in R (R version 4.3.1, R Core Team 2023, Vienna, AT) and RStudio (2023.06.1+524). The reported R^2 values always refer to the adjusted R^2. If not stated otherwise, the 'ggplot2' (Wickham 2009) and the 'cowplot' package (Wilke 2020) were used for visualizations.

2.7.1 Modeling of $\delta^2H_{Lipid1/Lipid2}$ values

We simulated algal $\delta^2H_{Lipid1/Lipid2}$ values with a 50,000 iteration Monte Carlo model based on the hydrogen isotope fractionation between different algal lipids and source water ($\alpha^2_{Lipid/Water}$) calculated from previously published culture experiments as well as the relative contribution of each algal group to the lipid pool based on the respective biovolume. Detailed model specifications for the modeling of biweekly $\delta^2H_{Lipid1/Lipid2}$ values can be found in the R code available in GitHub (https://github.com/antoniaKlatt/Klatt_etal_2024_phytoplankton_Rotsee).

Specifically, theoretical normal distributions of $\alpha^2_{Lipid/Water}$ values were estimated for each algal group and lipid based on mean $\alpha^2_{C16:0\ Acid/Water}$, $\alpha^2_{Sterol/Water}$ and $\alpha^2_{Phytol/Water}$ values with

corresponding standard deviations (SD) derived from batch cultures of *Cyanophyceae*, green algae, *Bacillario-, Dino-, and Cryptophyceae* (Ladd *et al.,* 2025; Pilecky *et al.,* 2024) (Fig. S4). $\alpha^2_{C16:0\ Acid/Water}$ values from Pilecky et al. (2024) were calculated based on $\delta^2H_{C16:0\ Acid}$ and δ^2H_{Water} values of single cultures excluding ^2H-enriched water. No $\alpha^2_{Sterol/Water}$ values were defined for *Cyanophyceae* as cyanobacteria do not produce any sterols (e.g., Volkman 2003; Martin-Creuzburg *et al.,* 2008; Taipale *et al.,* 2016; Peltomaa *et al.,* 2023). Due to missing $\alpha^2_{Sterol/Water}$ and $\alpha^2_{Phytol/Water}$ values, $\alpha^2_{Sterol/Water}$ and $\alpha^2_{Phytol/Water}$ distributions of *Chrysophyceae*were simulated based on $\alpha^2_{Lipid/Water}$ values from *Bacillario*- and *Dinophyceae* according to their phylogenetic relationship (Not *et al.,* 2021).

The three sets of α values predicted from each Monte Carlo simulation were then used to predict sets of $^2H/^1H_{Lipid}$ values for each lipid and algal group based on the $^2H/^1H_{Water}$ value at each sampling date. Then, biovolume-weighted average $^2H/^1H_{Lipid}$ values were calculated for each sampling date by the relative contribution of each algal group to the total phytoplankton biomass for C16:0 and phytol, and the relative contribution of each eukaryotic algal group to total eukaryotic algal biomass for sterols. The three sets of biovolume-weighted average $^2H/^1H$ values for each lipid were then used to calculate $\delta^2H_{C16:0\ Acid/Phytol\ phyto}$, $\delta^2H_{C16:0\ Acid/Sterol\ phyto}$ and $\delta^2H_{Sterol/Phytol\ phyto}$ values for each sampling date.

To model the potential impact of heterotrophic microzooplankton on $\delta^2H_{Lipid1/Lipid2}$ values, we conducted an additional 50,000 iteration Monte Carlo simulation to estimate theoretical hydrogen isotope fractionation factors between algal and microzooplankton lipids. For this purpose, we used observations of $\delta^2H_{C16:0\ Acid}$ values of seston and zooplankton from Pilecky *et al.* (2022) (Fig. S5) and calculated $\alpha^2_{seston/zoo}$ values. In this study, seston refers to dietary plankton of < 30 µm from eutrophic ponds (Pilecky *et al.,* 2022) which we used to represent phytoplankton in our calculations. Since empirical δ^2H_{sterol} values from zooplankton were not available, we applied the same set of fractionation factors between seston and zooplankton as that for C16:0 fatty acid.

We then simulated $^{2}H/^{1}H_{C16:0\ Acid}$ and $^{2}H/^{1}H_{Sterol}$ values from microzooplankton using biovolume-weighted $^{2}H/^{1}H_{Lipid}$ values from phytoplankton and the theoretical $\alpha^{2}_{seston/zoo}$ values. Subsequently, biovolume-weighted $^{2}H/^{1}H_{C16:0\ Acid}$ and $^{2}H/^{1}H_{Sterol}$ values from both phytoplankton and microzooplankton ($^{2}H/^{1}H_{Lipid\ phyto\&zoo}$) were calculated by the relative contribution to total biomass or eukaryotic biomass. Then, $\delta^{2}H_{Lipid1/Lipid2}$values representing theoretical contributions from algae and microzooplankton ($\delta^{2}H_{Lipid1/Lipid2\ phyto\&zoo}$) were computed using $^{2}H/^{1}H_{Lipid\ phyto\&zoo}$ values.

Seasonal and annual $\delta^{2}H_{Lipid1/Lipid2}$ values were calculated with a similar approach to biweekly simulations, but were modified to use seasonal or annual biovolume contributions, and seasonal or annual average water $\delta^{2}H$ values. Detailed model settings for the annual and seasonal calculations are specified in the R code which is available in GitHub (https://github.com/antoniaKlatt/Klatt_etal_2025_phytoplankton_Rotsee). Average $\delta^{2}H_{Lipid1/Lipid2}$values from winter 2019 include samples from January and February 2019, while values from winter 2020 include samples from December 2019, January, and February 2020. If no $\delta^{2}H_{Lipid}$ value was measurable, the lipid concentration at the specific sampling date was set to zero.

2.7.2 Lipid ratios

Lipid ratios were calculated based on initial lipid concentrations in the water column [µg/L].

Phytol:sterol ratios were calculated as:

[phytol]/([phytol] +[brassicasterol]+[ergosterol]+[sitosterol]+[stigmasterol]) (1),

and C18:C16 ratios were calculated as:

([C18:1]+[C18:x]+[C18:2]+[C18:3nx])/([C16:0]+[C18:1]+[C18:x]+[C18:2]+[C18:3nx]) (2)

where C18:x represents C18:1n9c co-eluting with C18:2n6t and C18:3nx is C18:3n3 with C18:3n6.

2.7.3 Statistical analyses

Spearman's correlation coefficients between $\delta^2H_{Lipid1/Lipid2}$values and the relative biovolume of different phytoplankton groups were calculated using the 'corr.test' function of the 'psych' package (Revelle, 2024) with a Bonferroni adjustment. Correlation matrices were visualized with the 'ggcorrplot' package (Kassambara 2023). Paired two-sided t-tests between modeled $\delta^2H_{Lipid1/Lipid2}$ values were performed with the 't.test' function from the 'stats' package (R Core Team 2023, Vienna, AT). Non-metric multidimensional scaling (NMDS) of relative alcohol and fatty acid concentrations was performed with the 'metaMDS' function of the 'vegan' package (Oksanen *et al.,* 2022) based on Bray-Curtis dissimilarities. Relative concentrations are based on the contribution of individual alcohols to the sum concentrations of all alcohols (excluding cholesterol) on single sampling dates, and the contribution of individual fatty acids to the sum concentrations of all fatty acids (excluding C22:2) on single sampling dates. NMDS of relative alcohol concentrations was performed with untransformed data, while relative fatty acid concentrations were square root transformed due to the strong 'arch' effect (Podani & Miklós 2002) produced by untransformed fatty acid concentrations. Redundancy Analysis (RDA) between phytoplankton biovolume and environmental variables was performed with the 'rda' function of the 'vegan' package (Oksanen *et al.,* 2022) without scaling of biovolume data. Relative biovolume of phytoplankton groups was square root transformed and total phosphorous concentrations were log transformed prior to RDA. Pearson's correlation between environmental variables were calculated using the 'corr.test' function of the 'psych' package (Revelle 2024). All statistical analyses were performed with complete datasets after removing complete rows containing non-values.

3. Results

3.1 Stratification and vertical mixing in Rotsee

The timing of lake stratification and the onset of autumnal mixing in monomictic Rotsee were assessed by the oxygen and temperature profiles in the water column (Fig. S2). The lake stratification began in spring, and a stable oxycline and thermocline was established between ~ 5 to 10 m depth in summer. Mixing began in October, deepening the thermocline, and no vertical stratification was present by December.

3.2 The phytoplankton community is highly dynamic

During the one-year sampling period, diatoms (*Bacillariophyceae*), green algae (*Chloro-* and *Zygnemophyceae*), golden algae (*Chrysophyceae*), cryptomonads (*Cryptopyceae*), cyanobacteria (*Cyanophyceae*), and dinoflagellates (*Dinophyceae*) were identified in varying abundance in Rotsee (Fig. 1). Some phytoplankton blooms were detected concurrently at both sampling depths, for instance, the winter diatom bloom in January 2019, or the major spring bloom of golden algae in April 2019 (Fig. 1A, B). However, some algal blooms were restricted to a certain sampling depth. For example, at 1 m depth, a smaller green algal bloom was detected in February 2019, and a bloom of cryptomonads in late June 2019 (Fig. 1A). At the chlorophyll maximum depth, a first cyanobacterial bloom occurred in late July 2019, followed by a bloom of photosynthetic dinoflagellates in mid-August (Fig. 1B). In October 2019, a massive second cyanobacterial bloom was detected (Fig. 1B), partly overlapping with the lake turnover event (Fig. S2). The cyanobacterial bloom in late October produced the highest absolute algal biovolume during the year.

Besides phytoplankton, various microzooplankton groups were identified, including Ciliata and Rotifera species, as well as the phagocytotic non-photosynthetic dinoflagellate *Gymnodinium helveticum* (Irish 1979; Wille & Hoffmann 1991) (Fig. 1). At 1 m depth, a massive peak of microzooplankton was detected in late July 2019, with Rotifera reaching

their maximum biovolume, followed by a Ciliata peak in August (Fig. 1A). The biovolume of Ciliates further increased in late October and mid-December (Fig. 1A). At the chlorophyll maximum depth, a Ciliata peak was detected in February 2019, followed by a massive increase of Ciliates in mid-June (Fig. 1B). The biovolume of *Gymnodinium helveticum* was generally low throughout the year.

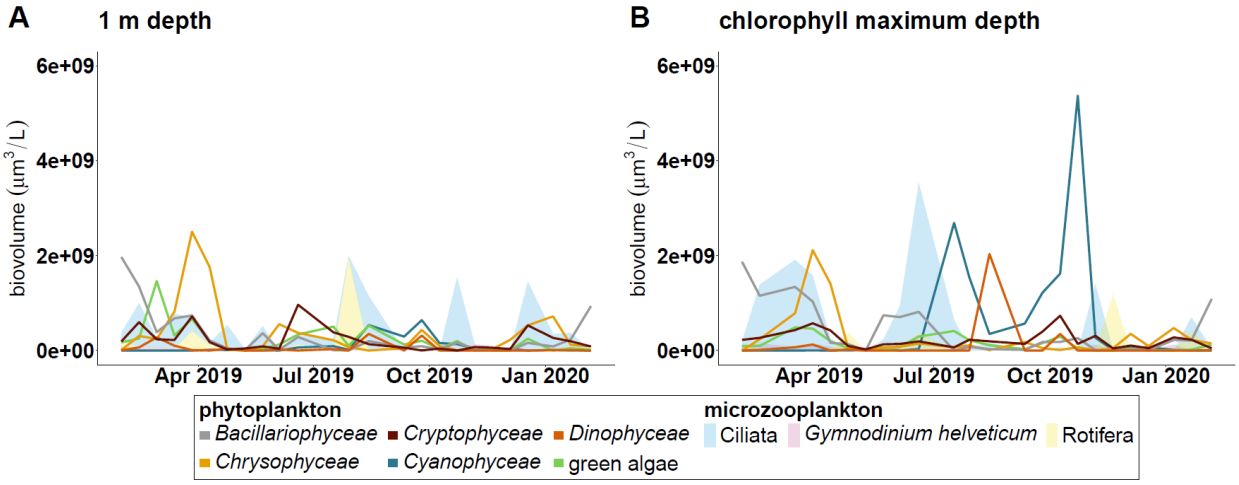

Figure 1: Absolute biovolume of phytoplankton and microzooplankton groups in Rotsee at 1 m depth (A) and chlorophyll maximum depth (B) over time. *Chlorophyceae* and *Zygnemophyceae* were included in the classification 'green algae'.

3.3 δ^2H_{Lipid} values generally do not correlate with δ^2H_{Water} values

To examine the potential impact of the isotopic signature of lake water on algal δ^2H_{Lipid} values in Rotsee, we compared changes of $\delta^2H_{C16:0\ Acid}$ and δ^2H_{Phytol} values with δ^2H_{Water} values (Fig. 2). δ^2H_{Lipid} values were much more variable than δ^2H_{Water} values. Overall, $\delta^2H_{C16:0\ Acid}$ values spanned a range > 100 ‰ (-304 to -163 ‰) and δ^2H_{Phytol} values > 60 ‰ (-434 to -373 ‰), while δ^2H_{Water} values only varied between -83 and -76 ‰. While $\delta^2H_{C16:0\ Acid}$ values were significantly positively correlated with δ^2H_{Water} values ($R^2 = 0.09$, $p < 0.05$) (Fig. 2A), δ^2H_{Phytol} values were not correlated with δ^2H_{Water} values (Fig. 2B).

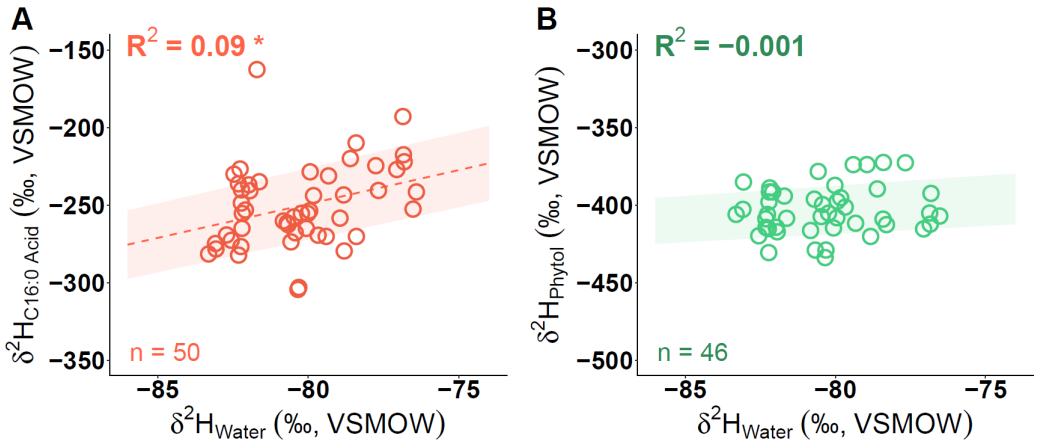

454

455 **Figure 2:** Linear regressions between δ^2H_{Water} and $\delta^2H_{C16:0\ Acid}$ values (A) and between δ^2H_{Water} and δ^2H_{Phytol}
456 values (B) in Rotsee. Shading represents 95 % confidence interval of the linear regression. *: P < 0.05.

457 Due to low concentrations, δ^2H measurements of sterols were only possible from a
458 subset of sampling dates. The greatest number of measurements were possible from
459 brassicasterol and sitosterol (Fig. S6). Sitosterol was generally the most ^2H-enriched sterol,
460 with δ^2H values ranging from -330 to -216 ‰. The most ^2H-depleted sterol was
461 brassicasterol, which had δ^2H values that ranged from -374 to -286 ‰. δ^2H_{Sterol} values were
462 generally not correlated with δ^2H_{Water} values, with the exception of stigmasterol (R^2 = 0.28, p
463 < 0.05).

464

465 ### 3.4 Biweekly relationships between $\delta^2H_{Lipid1/Lipid2}$ values and
466 ### phytoplankton community composition

467 To assess the fidelity of algal δ^2H_{Lipid} values as a proxy for phytoplankton community
468 assemblages, $\delta^2H_{Lipid1/Lipid2}$ values were calculated and the relationship between $\delta^2H_{Lipid1/Lipid2}$
469 values and algal community dynamics was analyzed. For late August 2019 and mid-February
470 2020, no phytoplankton cell counts were available. Due to the small size of our dataset,
471 highly dynamic phytoplankton fluctuations (Fig. 1) and difficulties of extrapolation (Hastie *et*
472 *al.,* 2009), algal biovolume was not inter-/extrapolated and corresponding lipid samples were
473 excluded from analyses. Moreover, due to missing δ^2H values of different sterols for many

sampling dates (Fig. S6), $\delta^2H_{C16:0\ Acid/Sterol}$ and $\delta^2H_{Sterol/Phytol}$ values were calculated with weighted average δ^2H_{Sterol} values of each sampling date.

There were no significant correlations between $\delta^2H_{Lipid1/Lipid2}$ values and the relative biovolume of individual phytoplankton groups, but the direction of some relationships was consistent at both sampling depths (Fig. S7, S8). For instance, green algal biovolume tended to increase with $\delta^2H_{C16:0\ Acid/Phytol}$ values (Fig. S7) and diatom biovolume tended to increase with $\delta^2H_{Sterol/Phytol}$ values (Fig. S8).

To assess if phytoplankton community shifts were reflected by $\delta^2H_{Lipid1/Lipid2}$ values, the relative biovolume of individual algal groups was combined based on similarities of $\delta^2H_{Lipid1/Lipid2}$ values in culturing studies (Ladd *et al.,* 2025; Pilecky *et al.,* 2024) and relationships found in Rotsee (Fig. S7, S8). No relationship between $\delta^2H_{C16:0\ Acid/Phytol}$ values and the summed biovolume of cyanobacteria and green algae was found (R^2 = -0.02, p = 0.6; Fig. S7). However, the summed biovolume of diatoms and golden algae was negatively correlated with $\delta^2H_{C16:0\ Acid/Sterol}$ values (R^2 = 0.11, p < 0.05) (Fig. 3A) and positively correlated with $\delta^2H_{Sterol/Phytol}$ values (R^2 = 0.24, p < 0.01) (Fig. 3B). When the linear regressions for these relationships were extrapolated to 100 % diatoms and golden algae, $\delta^2H_{C16:0\ Acid/Sterol}$ values were similar to measurements from diatom cultures (Ladd *et al.*, 2025) and were within 1 SD for $\delta^2H_{Sterol/Phytol}$ values (Fig. 3B).

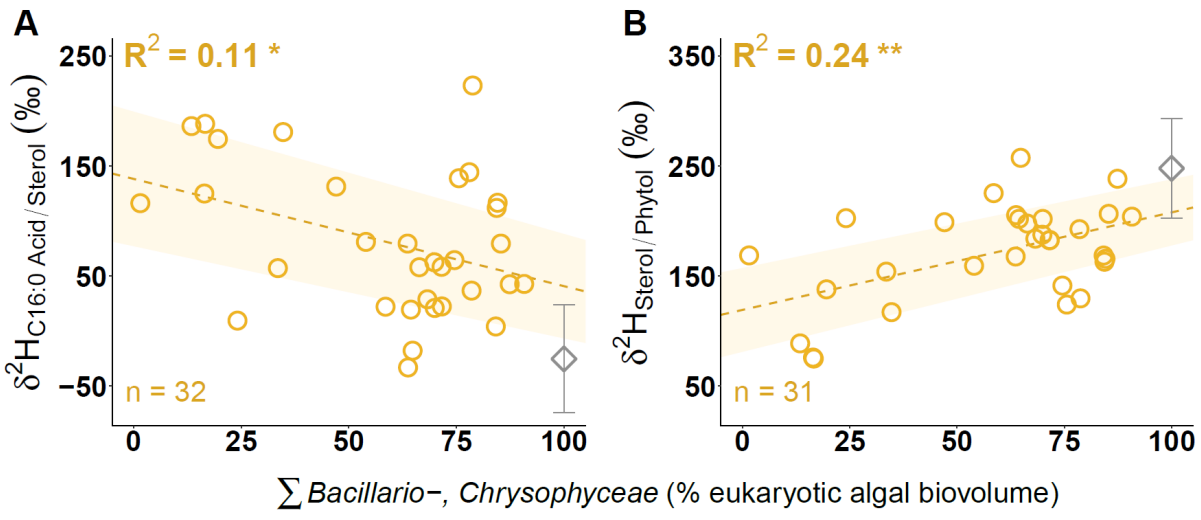

493 **Figure 3:** Linear regressions between $\delta^2H_{C16:0\ Acid/Sterol}$ (A) and $\delta^2H_{Sterol/Phytol}$ values (B) and the summed
494 relative biovolume of *Bacillario*- and *Chrysophyceae* in Rotsee. Diamond symbols indicate mean $\delta^2H_{C16:0\ Acid/Sterol}$
495 and $\delta^2H_{Sterol/Phytol}$ values from *Bacillariophyceae* cultures (Ladd et al., 2025), representing theoretical $\delta^2H_{Lipid1/Lipid2}$
496 values at 100% contribution to eukaryotic biovolume. Shading represents 95 % confidence intervals of the linear
497 regressions. *: $P < 0.05$; **: $P < 0.01$.

498 To further assess the impact of phytoplankton community composition on $\delta^2H_{Lipid1/Lipid2}$
499 values, measured $\delta^2H_{Lipid1/Lipid2}$ values were compared to modeled $\delta^2H_{Lipid1/Lipid2}$ values
500 exclusively derived from phytoplankton ($\delta^2H_{Lipid1/Lipid2\ phyto}$) (Fig. 4,5), which were simulated
501 based on theoretical δ^2H_{Lipid} values of individual algal groups (Ladd *et al.,* 2025; Pilecky *et al.,*
502 2024) and their biovolume in Rotsee. Moreover, the influence of microzooplankton on the
503 lipid isotopic signal was investigated by simulating $\delta^2H_{Lipid1/Lipid2}$ values incorporating
504 biovolume-weighted δ^2H_{Lipid} values of phytoplankton and microzooplankton ($\delta^2H_{Lipid1/Lipid2}$
505 $_{phyto\&zoo}$). Compared to phytoplankton lipids, lipids of heterotrophs are expected to be more
506 ^{2}H-enriched (e.g., X. Zhang *et al.* 2009; Pilecky *et al.,* 2022) and therefore, high
507 microzooplankton biovolume could potentially affect $\delta^2H_{Lipid1/Lipid2}$ values.

508 On a biweekly scale, mean values of modeled $\delta^2H_{Lipid1/Lipid2\ phyto}$ and $\delta^2H_{Lipid1/Lipid2\ phyto\&zoo}$
509 values were similar to each other for most sampling dates (Fig. 4). Larger differences were
510 found during peaks of microzooplankton biovolume, and were most pronounced for modeled
511 $\delta^2H_{C16:0\ Acid/Phytol}$ and $\delta^2H_{Sterol/Phytol}$ values. For instance, mean $\delta^2H_{Sterol/Phytol\ phyto\&zoo}$ values were
512 > 40 ‰ higher than mean $\delta^2H_{Sterol/Phytol\ phyto}$ values during Ciliata and Rotifera peaks in late
513 October and November.

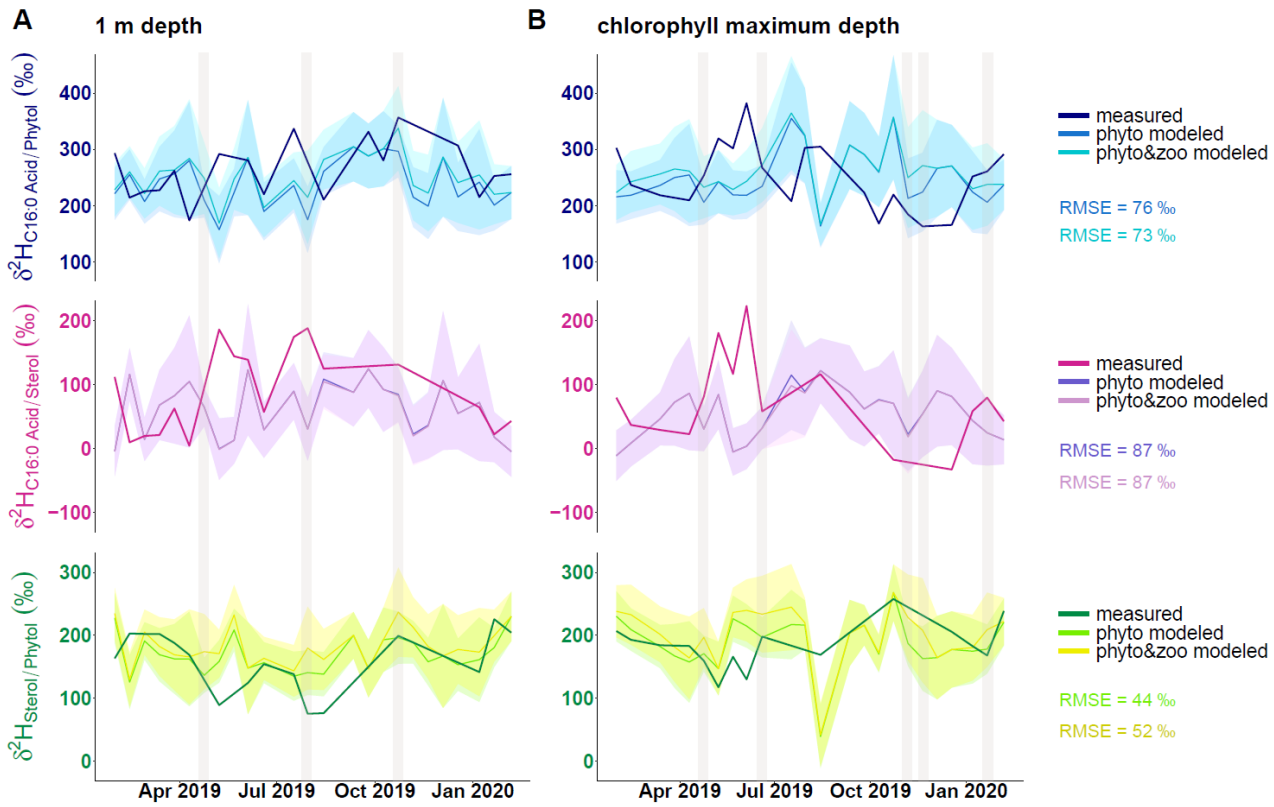

514

515 **Figure 4:** Biweekly comparison of modeled and measured $\delta^2H_{Lipid1/Lipid2}$ values in Rotsee at 1 m depth (A) and
516 chlorophyll maximum depth (B). Modeled $\delta^2H_{Lipid1/Lipid2}$ values were calculated incorporating weighted $^2H/^1H_{Lipid}$
517 values of autotrophic phytoplankton only ($\delta^2H_{Lipid1/Lipid2\ phyto}$) and a combination of weighted $^2H/^1H_{lipid}$ values from
518 autotrophic phytoplankton and heterotrophic microzooplankton ($\delta^2H_{Lipid1/Lipid2\ phyto\&zoo}$). For each sampling date, the
519 mean value of modeled $\delta^2H_{Lipid1/Lipid2}$ values is shown with the respective standard deviation indicated by shaded
520 areas. Root Mean Square Errors (RMSE) were calculated between measured $\delta^2H_{Lipid1/Lipid2}$ values and the mean
521 of modeled $\delta^2H_{Lipid1/Lipid2}$ values for each sampling date at both depths. Vertical shaded areas represent
522 microzooplankton biovolume peaks (> 50 % of total biovolume).

523 Measured $\delta^2H_{Lipid1/Lipid2}$ values were nearly identical to the mean of modeled $\delta^2H_{Lipid1/Lipid2}$
524 values on several sampling dates and mostly fell within 1 SD interval. However, larger
525 deviations between measured and modeled $\delta^2H_{Lipid1/Lipid2}$ values were found on single
526 sampling dates for all lipid pairs, particularly in early June. Further discrepancies were found
527 in May, when measured $\delta^2H_{C16:0\ Acid/Sterol}$ values exceeded the SD interval of modeled $\delta^2H_{C16:0}$
528 $_{Acid/Sterol}$ values by > 130 ‰ (Fig. 4A), and in mid-August, when measured $\delta^2H_{Sterol/Phytol}$ values
529 were nearly 80 ‰ higher than the SD interval of modeled values (Fig. 4B).

3.5 Yearly and seasonal relationships between $\delta^2H_{Lipid1/Lipid2}$ values and phytoplankton community composition

To analyze whether $\delta^2H_{Lipid1/Lipid2}$ values on a long-term scale reflect phytoplankton communities and microzooplankton contribution, yearly and seasonal $\delta^2H_{Lipid1/Lipid2\ phyto}$ and $\delta^2H_{Lipid1/Lipid2\ phyto\&zoo}$ values were modeled and compared to measured amount-weighted average $\delta^2H_{Lipid1/Lipid2}$ values (Fig. 5).

Annual and seasonal $\delta^2H_{Lipid1/Lipid2\ phyto}$ and $\delta^2H_{Lipid1/Lipid2\ phyto\&zoo}$ values were significantly different from each other for all lipid pairs (paired two-sided t-test; $p < 0.0001$), even though the size of this effect was generally small (Fig. 5). On the annual scale, the means of $\delta^2H_{C16:0\ Acid/Sterol}$ values were nearly identical between models (Fig. 5B), while for $\delta^2H_{C16:0\ Acid/Phytol}$ and $\delta^2H_{Sterol/Phytol}$ values, $\delta^2H_{Lipid1/Lipid2\ phyto\&zoo}$ values were ~ 15 and 17 ‰ higher than $\delta^2H_{Lipid1/Lipid2\ phyto}$ values (Fig. 5A, C). Seasonally, $\delta^2H_{Sterol/Phytol}$ values displayed the largest difference between models, with mean $\delta^2H_{Sterol/Phytol\ phyto\&zoo}$ values being up to ~ 22 ‰ higher than $\delta^2H_{Sterol/Phytol\ phyto}$ values (Fig. 5C).

On the annual scale, measured $\delta^2H_{Lipid1/Lipid2}$ values fell within 1 SD interval of modeled $\delta^2H_{Lipid1/Lipid2}$ values for all lipid pairs (Fig. 5), but measured $\delta^2H_{C16:0\ Acid/Phytol}$ and $\delta^2H_{Sterol/Phytol}$ values were > 30 ‰ lower than the mean of modeled $\delta^2H_{Lipid1/Lipid2\ phyto\&zoo}$ values (Fig. 5A, C). Measured $\delta^2H_{Lipid1/Lipid2}$ values were also within 1 SD of modeled values for most lipid pairs in most seasons (Fig. 5). However, there were some discrepancies between measured and modeled $\delta^2H_{Lipid1/Lipid2}$ values on the seasonal scale, particularly in autumn.

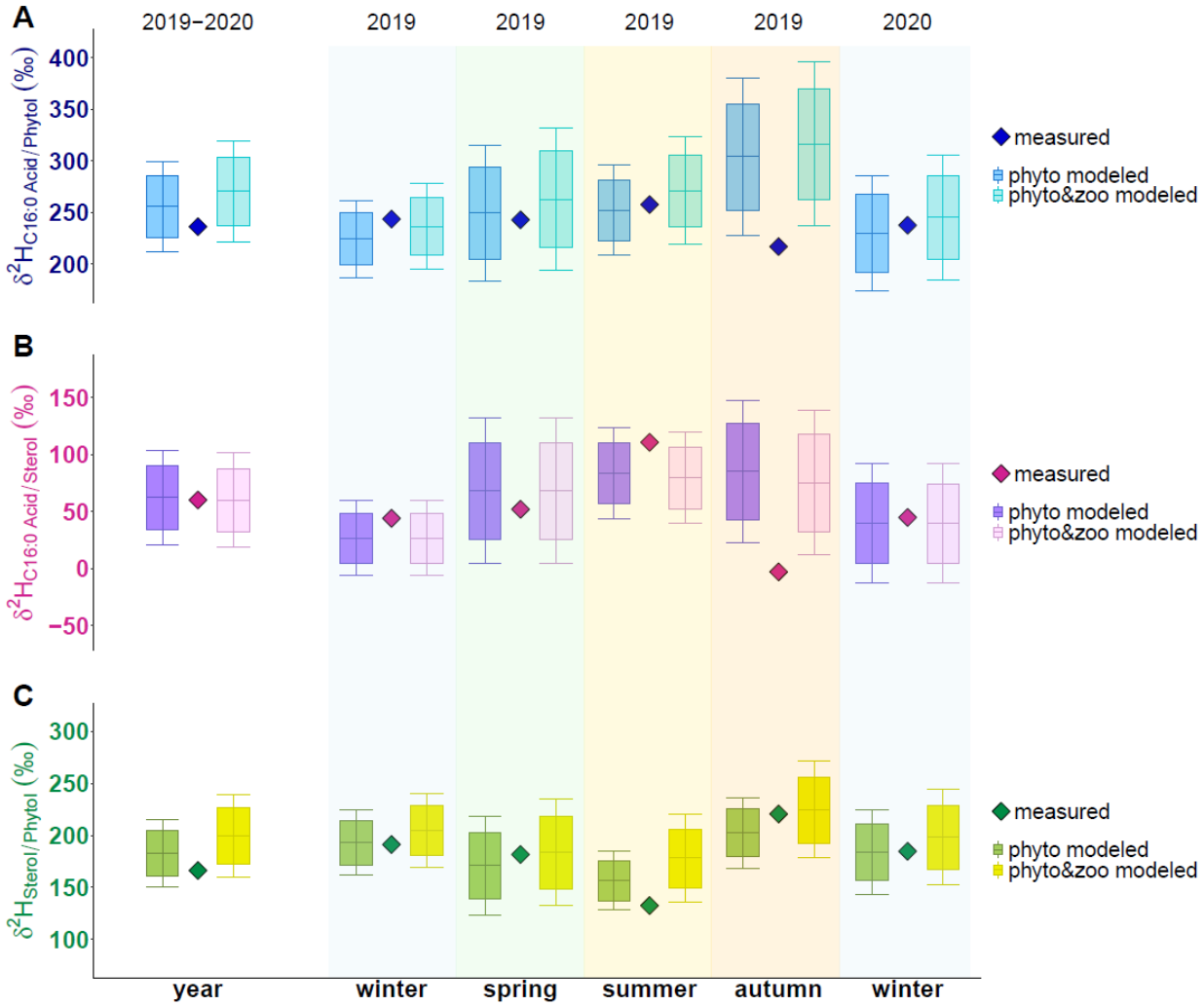

Figure 5: Comparison of modeled and measured weighted average $\delta^2H_{Lipid1/Lipid2}$ values in Rotsee over the year (2019-2020) and during meteorological seasons. Modeled $\delta^2H_{Lipid1/Lipid2}$ values were calculated incorporating weighted $^2H/^1H_{lipid}$ values of autotrophic phytoplankton only ($\delta^2H_{Lipid1/Lipid2\ phyto}$) and a combination of weighted $^2H/^1H_{lipid}$ values from autotrophic phytoplankton and heterotrophic microzooplankton ($\delta^2H_{Lipid1/Lipid2\ phyto\&zoo}$). Boxplots indicate the mean of modeled $\delta^2H_{Lipid1/Lipid2}$ values with the respective standard deviation. Single rows indicate yearly and seasonal modeled and measured $\delta^2H_{C16:0\ Acid/Phytol}$ (A), $\delta^2H_{C16:0\ Acid/Sterol}$ (B), and $\delta^2H_{Sterol/Phytol}$ values (C).

3.6 Phytol:sterol ratios and C18:C16 ratios correlate with cyanobacterial biovolume

Alcohols included phytol, diplopterol (hopan-22-ol), brassicasterol, cholesterol (cholest-5-en-3β-ol), ergosterol (methylcholesta-5,7,22-trien-3β-ol), sitosterol, and stigmasterol (Fig.

563 S9). Cholesterol was excluded from further analysis due to its common abundance in
564 zooplankton (e.g., Goad 1981; Serrazanetti *et al.*, 1992; Wittenborn et al., 2020). The acid
565 fractions contained different saturated and unsaturated fatty acids potentially indicative for
566 phytoplankton including C14:0, C16:0, C16:1, C18:0, C18:1, C18:x, C18:2, C18:3nx,
567 C20:3nx, C20:4, C22:2 and C22:6 (Fig. S10), where C20:3nx is C20:3n3 with C20:3n6.
568 C22:2 was excluded from analysis due to its abundance at only one sampling date (Fig.
569 S10). Samples further contained trace amounts of C15:0, C17:0 and C17:1 fatty acids, which
570 were not quantified, with the exception of two samples derived from late July (2019-07-29)
571 and mid-September (2019-09-11), when C17:1 fatty acid increased to 2.9 and 3.3 µg/L at the
572 chlorophyll maximum depth. However, due to their general low abundance and likely
573 bacterial origin (e.g., Killops & Killops 2004), C15:0, C17:0 and C17:1 were not included in
574 further analyses.

575 To analyze (dis-)similarities of lipid distributions among samples in relation to
576 phytoplankton community changes, NMDS of relative alcohol concentrations and relative
577 fatty acid concentrations was performed, with visualization of relative cyanobacterial
578 biovolume at each sampling date (Fig. S11). There was a clear separation of samples with
579 high sterol concentrations from samples with high phytol concentrations along NMDS axis 1
580 (Fig. S11A), with the highest phytol concentrations co-occurring with cyanobacterial blooms.
581 In the analysis of fatty acid abundance, saturated compounds were separated from
582 unsaturated fatty acids along NMDS axis 1 (Fig. S11B). Cyanobacterial blooms co-occurred
583 with high concentrations of C16:1, C18:1, and C20:3nx, and rather high concentrations of
584 C18:2, C18:3nx, and C18:x.

585 Following NMDS analyses (Fig. S11), we calculated phytol:sterol ratios and C18:C16
586 ratios (eq. 1 & 2) in the water column of Rotsee and analyzed their relationship with
587 cyanobacterial biovolume (Fig. 6).

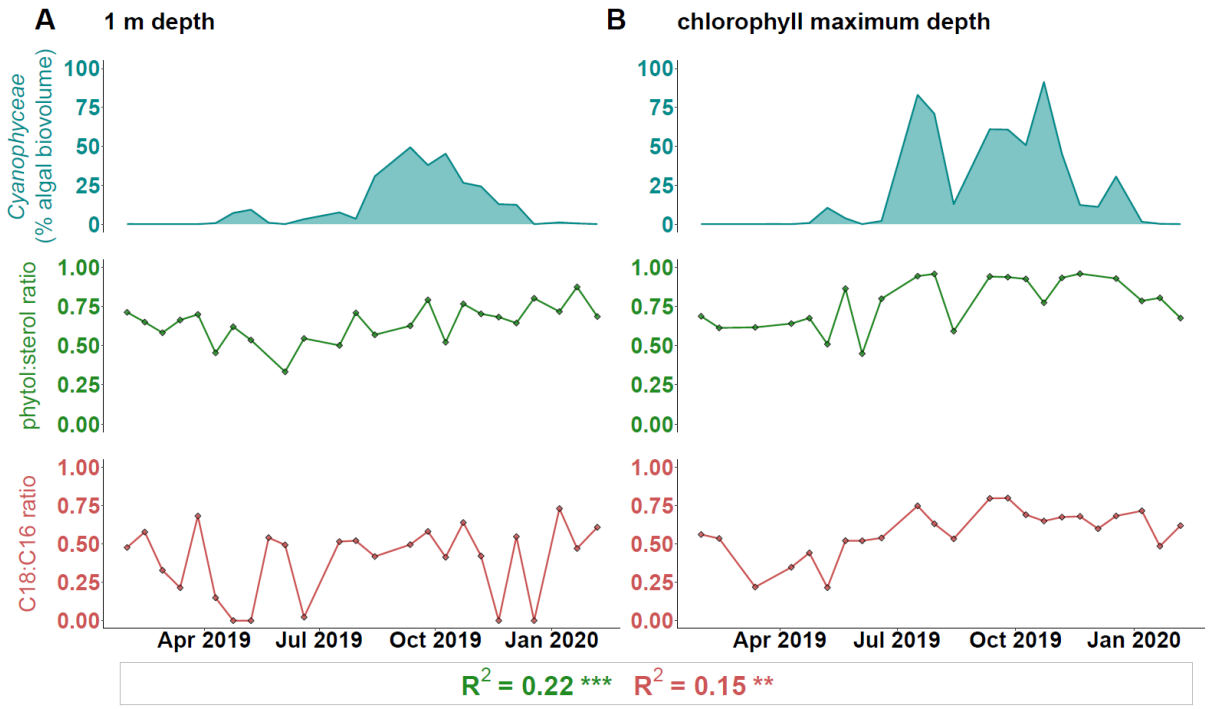

588

589 **Figure 6:** Time series of relative cyanobacterial biovolume, phytol:sterol ratios and C18:C16 ratios in Rotsee
590 at 1 m depth (A) and chlorophyll maximum depth (B). R^2 values refer to linear regressions between phytol:sterol
591 ratios and cyanobacterial biovolume, as well as C18:C16 ratios and cyanobacterial biovolume analyzed for
592 combined sampling depths. **: P < 0.01; ***: P < 0.001.

593 At 1 m depth, cyanobacteria were generally not abundant, with the exception of a bloom
594 in September and October, where cyanobacterial biovolume increased to > 40 % of total
595 phytoplankton biovolume (Fig. 1; Fig. 6). During cyanobacterial blooms, phytol:sterol ratios
596 and C18:C16 ratios increased to > 0.5. At the chlorophyll maximum depth, cyanobacterial
597 blooms occurred in July and in September/October, with cyanobacterial biovolume
598 increasing to > 60 % and > 90 % of total algal biovolume (Fig. 1; Fig. 6). Phytol:sterol ratios
599 clearly increased during cyanobacterial blooms to > 0.9. C18:C16 also increased but to a
600 lesser extent, with a maximum of ~ 0.6 in late September (Fig. 6B). Cyanobacterial
601 biovolume was significantly positively correlated with both lipid ratios.

602

4. Discussion

We analyzed $\delta^2H_{Lipid1/Lipid2}$ values and the distribution of algal lipids in the water column of Rotsee in relation to phytoplankton community changes throughout a one-year sampling period. δ^2H_{Lipid} values had much greater variability than δ^2H_{Water} values (Fig. 2), suggesting that other factors besides δ^2H_{Water} values, such as the composition of the algal community, are more important in determining δ^2H_{Lipid} values. However, algal δ^2H_{Lipid} values could still be used as a proxy for δ^2H values of lake water as changes in the phytoplankton community could be disentangled from changes in past δ^2H_{Water} values by the comparison of δ^2H values of source-specific and generic lipids as suggested by Ladd *et al.* (2025).

In the following discussion, we evaluate hydrogen isotope offsets among lipids, specifically $\delta^2H_{C16:0\ Acid/Phytol}$, $\delta^2H_{C16:0\ Acid/Sterol}$, and $\delta^2H_{Sterol/Phytol}$ values, as potential indicators for phytoplankton community dynamics and lipid ratios as proxy for cyanobacterial biovolume. We discuss uncertainties in their interpretation and further consider their application in paleoecological contexts to reconstruct past phytoplankton community dynamics.

4.1 Evaluation of $\delta^2H_{Lipid1/Lipid2}$ values as indicators of phytoplankton community compositions

Relationships between biweekly $\delta^2H_{Lipid1/Lipid2}$ values and algal biovolume in Rotsee (Fig. S7, S6) were generally in accordance with previous culturing studies (Ladd *et al.,* 2025). During the cyanobacterial bloom in summer (71 % of algal biovolume) (Fig. 1B), $\delta^2H_{C16:0\ Acid/Phytol}$ values increased up to 302 ‰, consistent with high $\delta^2H_{C16:0\ Acid/Phytol}$ values from cyanobacterial cultures (351 +/- 99 ‰; Ladd *et al.,* 2025). Likewise, diatom blooms (> 75 % of eukaryotic algal biovolume) (Fig. 1) were associated with high $\delta^2H_{Sterol/Phytol}$ values (> 200 ‰) and low $\delta^2H_{C16:0\ Acid/Sterol}$ values (< 100 ‰), similar to diatom cultures (248 +/- 45 ‰ and -25 +/- 49 ‰; Ladd *et al.,* 2025). Therefore, $\delta^2H_{Lipid1/Lipid2}$ values might be indicative of specific algal groups if they form a dominant part within the phytoplankton community. Additionally,

changes in $\delta^2H_{C16:0\ Acid/Sterol}$ and $\delta^2H_{Sterol/Phytol}$ values might indicate shifts within the eukaryotic algal community, even if groups with similar $\delta^2H_{Lipid1/Lipid2}$ values, such as diatoms and golden algae, cannot be resolved from each other (Fig. 3).

Beside phytoplankton in Rotsee, heterotrophic microzooplankton represent another autochthonous lipid source within the water column (Fig. 1). δ^2H_{Lipid} values of heterotrophic organisms are expected to be higher than algal δ^2H_{Lipid} values as NAD(P)H derived from glycolysis or the oxidative pentose phosphate pathway (oxPPP) is ^{2}H-enriched compared to the extremely ^{2}H-depleted NADPH formed in photosystem I (PS I) (e.g., Schmidt *et al*., 2003; X. Zhang *et al.* 2009; Cormier *et al.*, 2018; Cormier *et al.,* 2022). To assess the potential impact of microzooplankton, we modeled $\delta^2H_{Lipid1/Lipid2\ phyto}$ and $\delta^2H_{Lipid1/Lipid2\ phyto\&zoo}$ values and compared modeling results with measured $\delta^2H_{Lipid1/Lipid2}$ values (Fig. 4, 5). While $\delta^2H_{Lipid1/Lipid2\ phyto}$ values solely incorporate biovolume-weighted δ^2H_{Lipid} values of phytoplankton groups derived from batch cultures (Ladd *et al*., 2025; Pilecky et al., 2024), $\delta^2H_{Lipid1/Lipid2\ phyto\&zoo}$ values additionally include theoretical biovolume-weighted $\delta^2H_{C16:0\ Acid}$ and δ^2H_{Sterol} values of microzooplankton. We accounted for the net impact of different NAD(P)H pools, dietary and water δ^2H values, as well as kinetic fractionation by enzymes during fatty acid synthesis (Solomon *et al.,* 2009; X. Zhang *et al.,* 2009; Vander Zanden *et al.,* 2016; Pilecky *et al*., 2022) by the application of an empirically derived fractionation factor between $\delta^2H_{C16:0\ Acid}$ values of seston and zooplankton (Pilecky *et al.,* 2022).

Although several microzooplankton peaks occurred throughout the year (Fig. 1), the RMSE of modeled $\delta^2H_{Lipid1/Lipid2\ phyto}$ and $\delta^2H_{Lipid1/Lipid2\ phyto\&zoo}$ values were mostly similar (Fig. 4A, B), supporting a generally minor isotopic impact of microzooplankton. This is in accordance with short-term ^{13}C-labelling experiments suggesting that Rotsee is net autotrophic (Lammers *et al.,* 2016).

Large discrepancies between biweekly measured and modeled $\delta^2H_{Lipid1/Lipid2}$ values are likely associated with the relatively small number of freshwater taxa from which culturing data were available (Ladd et al., 2025; Pilecky et al., 2024). For instance, various *Cryptomonas*

656 species compromising most of eukaryotic algal biovolume in early May (Fig. 1A) might be
657 poorly represented by δ^2H_{Lipid} values from batch cultures including only two different species
658 (Ladd et al., 2025; Pilecky et al., 2024).

659 On the seasonal scale, large differences between measured and modeled $\delta^2H_{C16:0\ Acid/Phytol}$
660 and $\delta^2H_{C16:0\ Acid/Sterol}$ values were particularly found in autumn (Fig. 5A, B) when cyanobacteria
661 were the most abundant algal group. There was also no relationship between $\delta^2H_{C16:0\ Acid/Phytol}$
662 values and cyanobacterial biovolume on the biweekly scale (Fig. S7), contrasting the
663 expectations from algal cultures (Ladd *et al.,* 2025).

664 During cyanobacterial blooms, increased cellular growth rates, which have been shown to
665 cause ^2H-depletion in lipids of some eukaryotic algae (e.g., Z. Zhang *et al.,* 2009; Sachs &
666 Kawka 2015), could impact $\delta^2H_{C16:0\ Acid/Phytol}$ values. This effect would be consistent with the
667 measured $\delta^2H_{C16:0\ Acid}$ value (-267 ‰) during the main cyanobacterial bloom in late October (>
668 90 % of algal biovolume) (Fig. 1B), which was at the lower end of values from cyanobacterial
669 batch cultures (-236 +/- 32 ‰; Ladd *et al.*, 2025).

670 The δ^2H_{Phytol} value (-399 ‰) was, however, more ^2H-enriched than expected from
671 culturing results (-433 +/- 18 ‰; Ladd *et al.*, 2025). A potential explanation for the ^2H-
672 enrichment of phytol could be mixotrophic cyanobacterial growth due to light limitation and
673 decreasing CO_2 concentrations (Zagarese *et al.,* 2021; Cormier *et al.,* 2022; Muñoz-Marín *et*
674 *al.,* 2024; Torres-Romero *et al.,* 2024), associated with higher relative proportions of ^2H-
675 enriched NADPH from glycolysis or the oxPPP (Cormier *et al.,* 2022). A potential isotopic
676 imprint of mixotrophy could be further indicated by the ^2H-enrichment of sitosterol and
677 stigmasterol during the bloom event of the mixotrophic dinoflagellate *Ceratium hirundinella*
678 (e.g., Callieri et al., 2006) (Fig. 1B), likely causing a large offset between measured and
679 modeled $\delta^2H_{Sterol/Phytol}$ values (Fig. 4B).

680 Finally, the main cyanobacterial bloom in late October overlapped with the initiation of the
681 autumnal lake mixing (Fig. S2), potentially transferring organic matter from the deeper
682 hypolimnion to the epilimnion. This could include ^2H-depleted fatty acids derived from sulfur
683 bacteria within the hypolimnion of Rotsee (Kohler et al., 1984; X. Zhang *et al.* 2009;

Heinzelmann et al., 2015b; Lammers et al., 2016). Together with the observed ^{2}H-enrichment of phytol, this could result in overall low $\delta^{2}H_{C16:0\ Acid/Phytol}$ values during autumn. The impact of the mixing event was also apparent in the phytol:sterol ratios, which had a stronger correlation with cyanobacterial biovolume when sampling dates during lake mixing were excluded (2019-10-09 to 2019-12-04) ($R^2 = 0.27$, $p < 0.001$).

Despite the high uncertainty of our modeling approach as well as the potential short-term impacts of algal metabolism and lake mixing on $\delta^{2}H_{Lipid1/Lipid2}$ values, measured $\delta^{2}H_{Lipid1/Lipid2}$ values were nearly identical to the mean of modeled algal $\delta^{2}H_{Lipid1/Lipid2\ phyto}$ values on multiple sampling dates (Fig. 4) and for multiple seasons (Fig. 5). Therefore, the fluctuations of phytoplankton community composition during the year are generally reflected by $\delta^{2}H_{Lipid1/Lipid2}$ values.

4.2 Lipid ratios as proxies for cyanobacterial biovolume

Besides $\delta^{2}H_{Lipid1/Lipid2}$values, we investigated lipid distributions in the water column in relation to phytoplankton biovolume. Phytol:sterol ratios were positively correlated with cyanobacterial biovolume ($R^2= 0.22$, $p < 0.001$) (Fig. S11, Fig. 6), in accordance with previous findings that most cyanobacteria do not produce any sterols (Martin-Creuzburg *et al.,* 2008; Taipale *et al.,* 2016; Peltomaa *et al.,* 2023). The co-occurrence of unsaturated C18 fatty acids with high cyanobacterial biovolume in Rotsee is consistent with the use of unsaturated C18 fatty acids as cyanobacterial biomarker (Bauersachs *et al*., 2017; Zeman-Kuhnert *et al.,* 2023). Although cyanobacterial biovolume was significantly positively correlated with the summed concentration of unsaturated C18 fatty acids ($R^2 = 0.28$, p-value < 0.0001), high concentrations of polyunsaturated C18 fatty acids have also been found in different green algae, as well as Chromalveolates (Taipale *et al.,* 2016; Lang *et al.,* 2011) and some cyanobacteria strains produce similar amounts of C16:0 and C18:3ω3 (Peltomaa *et al.,* 2023). Moreover, C16:0 and unsaturated C18 fatty acids might be additionally synthesized by bacteria, e.g., sulfur bacteria and methanotrophs (Bodelier et al., 2009;

711 Heinzelmann et al., 2015b; Lammers et al., 2016; Mayr et al., 2020) although bacterial
712 biomass tend to be generally lower than algal biomass in the water column of eutrophic lakes
713 (Coveney et al., 1977; Meinhard et al., 1992; Biddanda et al., 2001). Therefore, phytol:sterol
714 ratios might be more suitable as a cyanobacterial proxy since they are based on an exclusive
715 feature of cyanobacteria (the lack of sterol production), while C18:C16 ratios might be biased
716 by the additional incorporation of bacterial C16:0 and unsaturated C18 fatty acids from
717 eukaryotic algae. This is also indicated by the weaker correlation between C18:C16 ratios
718 and cyanobacterial biovolume (R^2= 0.15, $p < 0.01$) compared to phytol:sterol ratios (R^2= 0.22,
719 $p < 0.001$) (Fig. 6).

720 In general, phytol:sterol ratios and C18:C16 ratios might also be impacted by changes in
721 temperature, phosphorus and silicate availability which affect algal sterol and fatty acid
722 production rates (Piepho *et al.,* 2010; Piepho *et al.,* 2012; Matsui *et al.,* 2020; Calderini *et al.,*
723 2023). In Rotsee, water temperatures at different sampling depths ranged from 4 to 25 °C
724 and phosphorus concentrations ranged from 8 to 56 µg/L throughout the year (Fig. S12).
725 Only absolute concentrations of brassicasterol (R^2 = 0.14, $p < 0.01$) and C20:4 fatty acid (R^2
726 = 0.07, $p < 0.05$) (µg/L) were significantly negatively correlated with temperature, suggesting
727 a rather minor impact of temperature on lipid synthesis or no general trend among different
728 phytoplankton species as proposed by Piepho *et al.* (2012). However, concentrations of
729 C16:1 (R^2 = 0.2, $p < 0.001$), C18:2 (R^2 = 0.1, $p < 0.05$), C18:x (R^2 = 0.1, $p < 0.05$) and C18:1
730 (R^2 = 0.1, $p < 0.05$) were significantly positively correlated with total phosphorus
731 concentrations as well as phytol:sterol ratios (R^2 = 0.28, $p < 0.001$) and C18:C16 ratios (R^2 =
732 0.12, $p < 0.01$). Phytoplankton growth in eutrophic lakes is generally limited by phosphorus
733 (e.g., Liang et al., 2020; Jiang & Nakano 2022), and increasing phosphorus concentrations
734 can potentially promote cyanobacterial blooms (e.g., Huisman *et al*., 2018; Jankowiak *et al.*,
735 2019). Despite a collinearity between phosphorus, nitrogen and temperature in Rotsee,
736 relative cyanobacterial biovolume was positively associated with high phosphorus
737 concentrations (Fig. S13). Therefore, the significant correlation between lipid ratios and total
738 phosphorus concentrations is likely an indirect effect of phosphorus fertilization, while the

relationship between cyanobacteria and eukaryotic algae is the main driver of variability in lipid ratios.

4.3 $\delta^2H_{Lipid1/Lipid2}$ values and lipid ratios as paleoecological proxies for phytoplankton community dynamics

In the past, phytoplankton have greatly impacted Earth's climate (Kopp et al., 2005; Shen et al., 2018) and future changes in phytoplankton community composition could lead to alterations in biogeochemical cycles (Henson et al., 2021). In particular, the relationship between eukaryotic algae and cyanobacteria has been shown to impact carbon sequestration efficiency (Shen et al., 2018). In this context, reconstructions of past phytoplankton community dynamics in the sedimentary record comprise important context for future trajectories of algal communities (Shen et al., 2018; Cvetkoska *et al.,* 2021).

In our study, annually-integrated and amount-weighted $\delta^2H_{Lipid1/Lipid2}$ values are the most representative of a potential sedimentary isotopic signal, as sediment samples typically incorporate longer timescales. Annual $\delta^2H_{Lipid1/Lipid2}$ values in the water column of Rotsee were almost identical to modeled algal $\delta^2H_{Lipid1/Lipid2\ phyto}$ values (Fig. 5) indicating that $\delta^2H_{Lipid1/Lipid2}$ values mainly reflect phytoplankton community composition, while biases related to lake mixing and signatures of heterotrophic and/or mixotrophic δ^2H_{Lipid} values were averaged out.

Generally, annual $\delta^2H_{Lipid1/Lipid2}$ values in the water column of eutrophic lakes are expected to reflect algal community compositions, since larger mesoplankton comprise only ~ 1 to 5 % of phytoplankton biomass (Yuan & Pollard 2018) and the overall proportion of bacterial biomass is low (Coveney et al., 1977; Simon et al., 1992; Biddanda et al., 2001). However, in oligotrophic lakes with low nutrient availability and algal productivity, higher relative contributions from bacteria and zooplankton (Simon et al., 1992; Yuan & Pollard 2018) as well as from allochthonous sources, e.g., catchment vegetation, might attenuate the phytoplankton signal in $\delta^2H_{Lipid1/Lipid2}$ values and lipid ratios within the water column. Higher proportions of algal mixotrophy in oligotrophic lakes (Caron *et al.,* 1993; Pålsson & Granéli

765 2004; Saad *et al.,* 2016) might further complicate the application of $\delta^2H_{Lipid1/Lipid2}$ values as
766 phytoplankton proxy.

767 Independent from the trophic state of a lake, the transfer of organic matter from the water
768 column to the sediment is associated with lipid degradation (Meyers & Ishiwatari 1993;
769 Bechtel & Schubert 2009a,b). Degradation susceptibilities vary among algal lipids
770 (Kawamura *et al.,* 1987; Rontani & Volkman 2003; Martin-Creuzberg & von Elert 2004;
771 Peltomaa *et al*., 2017; Zeman-Kuhnert *et al.,* 2023), and could lead to ^2H-enrichment of lipids
772 in surface sediment relative to the water column (Gray *et al.,* 2002; Mancini *et al*., 2003;
773 Miljević & Golobočanin 2007; Sachs & Schwab, 2011; Schwab et al., 2015; Ladd *et al*., 2018)
774 or to changes in the relative abundance of different compounds. In particular, the relatively
775 fast mineralization of polyunsaturated C18 fatty acids compared to saturated fatty acids like
776 C16:0 (Kawamura *et al.,* 1987) likely compromises the significance of C18:C16 ratios as a
777 paleoecological proxy.

778 After incorporation into the sediment, the degradation of lipids has been shown to
779 generally decrease with increasing sediment depth. Higher sedimentation rates, anoxic
780 conditions and attachment to organic matter all favor lipid preservation (Meyers & Ishiwatari
781 1993; Harvey et al., 1996; Jeng *et al.,* 1997). Moreover, δ^2H values of carbon-bound
782 hydrogen are stable during early diagenesis (Schimmelmann *et al.,* 2006), preserving δ^2H_{Lipid}
783 values in the sediment.

784 Yet, non-algal sources of organic matter, specifically the microbial community within the
785 sediment, might alter sedimentary δ^2H_{Lipid} values and lipid ratios. The microbial activity in the
786 sediment generally increases with increasing trophic state (Wobus et al., 2003; Bechtel &
787 Schubert 2009b; Fiskal et al., 2019; Han et al., 2020), potentially associated with higher
788 bacterial contribution to sedimentary organic matter in eutrophic lakes (Bechtel & Schubert
789 2009b). In some cases, however, bacterial and archaeal abundance were comparable
790 between oligotrophic and eutrophic lakes (Wobus et al., 2003; Han et al., 2020). Despite the
791 higher microbial activity and potential higher bacterial contribution to organic matter, algal

792 contributions to the sedimentary lipid pool have been shown to still dominate microbial fatty
793 acids in eutrophic lakes (Heinzelmann *et al.,* 2018). To generally assess potential bacterial
794 sources of fatty acids in the sediment, other bacterial biomarkers like iso and anti-iso C15:0
795 and C17:1 fatty acid, as well as branched fatty acids and triterpenoid alcohols could be
796 analyzed (Kaneda 1991; Meyers & Ishiwatari 1993; Killops & Killops 2004; Bechtel &
797 Schubert 2009b). Likewise, the organic input from the catchment vegetation can be inferred
798 by organic carbon and nitrogen of bulk matter (Perdue & Koprivnjak 2007) and long-chain
799 saturated fatty acids (Bechtel & Schubert 2009b).

800 Regardless of the potential complications, sedimentary $\delta^2H_{Lipid1/Lipid2}$ values and lipid ratios
801 are a promising tool to increase the robustness of phytoplankton community reconstructions.
802 With an average sedimentation rate of 0.38 cm yr^{-1} in Rotsee (Naeher *et al.*, 2012), single
803 bloom events and seasonal variability cannot be inferred from $\delta^2H_{Lipid1/Lipid2}$ values and/or lipid
804 ratios in sediment samples. Nevertheless, major shifts towards dominant algal groups
805 averaging more than half of algal biovolume over several years and large phytoplankton
806 community changes over longer timescales might be reflected in the sediment record. For
807 instance, substantial impacts on the algal community associated with rising temperatures
808 during the Younger Dryas – Holocene transition or with recent lake eutrophication during the
809 20^{th} century (Stivrins et al., 2016; Hollander et al., 1992; Lotter 1998; Thevenon et al., 2012)
810 would be expected to produce changes in sedimentary $\delta^2H_{Lipid1/Lipid2}$ values.

811 In this context, downcore $\delta^2H_{C16:0\ Acid/Sterol}$ and $\delta^2H_{Sterol/Phytol}$ values could trace past shifts in
812 the eukaryotic algal community, with high $\delta^2H_{Sterol/Phytol}$ values (> 200 ‰) and low $\delta^2H_{C16:0\ Acid/Sterol}$
813 values (< 100 ‰) being indicative for a dominance of diatoms and/or golden algae
814 (Fig. 3, Fig. 7). Moreover, a co-occurrence of high $\delta^2H_{C16:0\ Acid/Phytol}$ values (> 250 ‰) and high
815 phytol:sterol ratios (> 0.75) can be expected during phases of high cyanobacterial and rather
816 low eukaryotic algal biomass (Fig. 7).

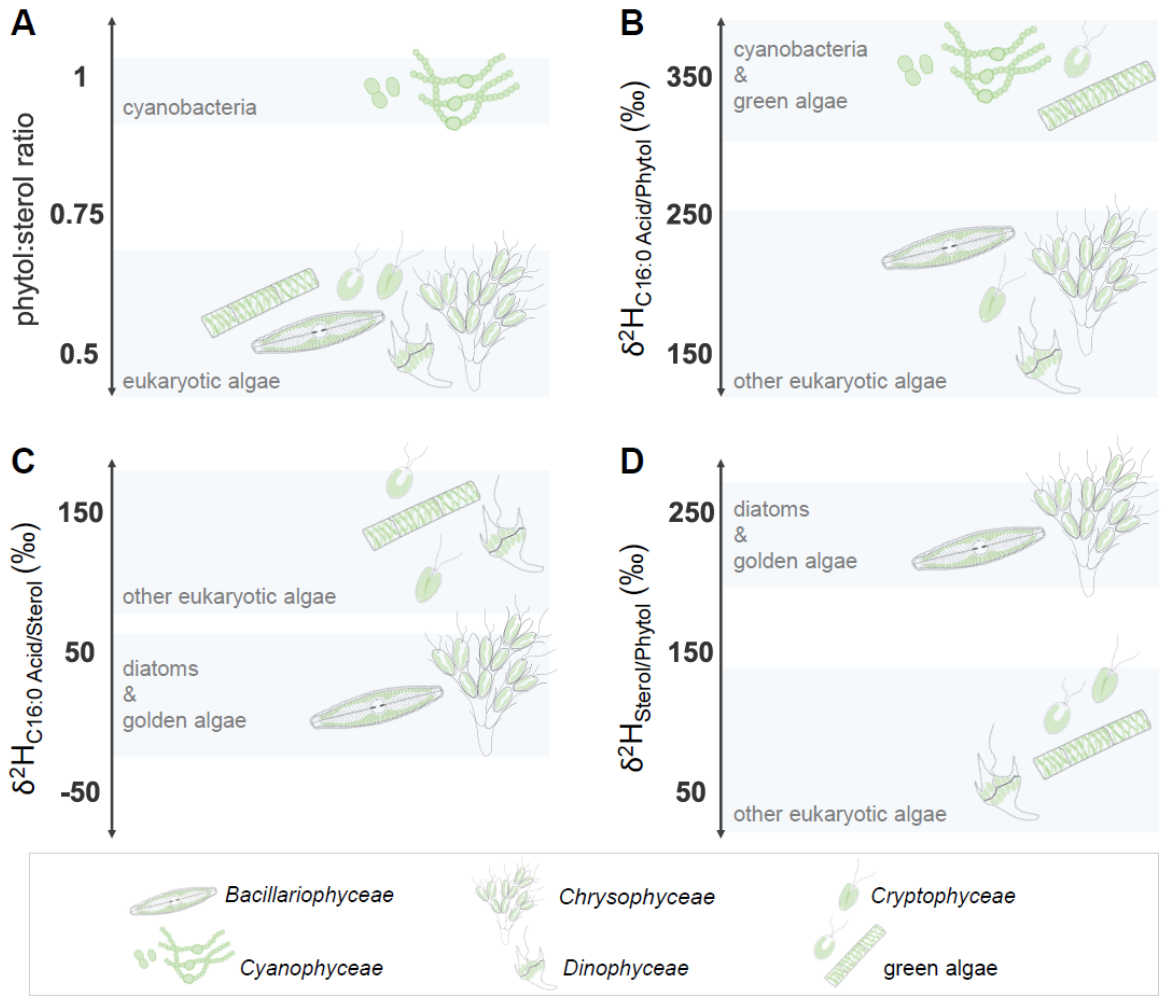

817

818 **Figure 7:** Schematic illustration of how phytol:sterol ratios (A), $\delta^2H_{C16:0\ Acid/Phytol}$ (B), $\delta^2H_{C16:0\ Acid/Sterol}$ (C), and
819 $\delta^2H_{Sterol/Phytol}$ (D) values could be used as proxies for phytoplankton community composition.

820 Additionally, the combination of $\delta^2H_{Lipid1/Lipid2}$ values and lipid ratios with proxies for
821 individual algal groups offers the opportunity to analyze past relationships between single
822 algal groups and the phytoplankton community. For instance, while diatom abundance and
823 species richness can be quantitatively inferred by their silica frustules, the additional analysis
824 of $\delta^2H_{C16:0\ Acid/Sterol}$ and $\delta^2H_{Sterol/Phytol}$ values would indicate if diatoms were dominant within the
825 phytoplankton community. The proportion of golden algae and diatoms could be further
826 disentangled by the ratio of diatom frustules and statospores of golden algae species (Smol
827 1985). Recently, *sed*aDNA approaches have been increasingly adopted to reconstruct past
828 cyanobacterial dynamics, also in combination with other algal proxies, e.g. sedimentary
829 pigments (e.g., Pal *et al.,* 2015; Cao *et al.*, 2020; Nwosu *et al.*, 2023). The application of

*sed*aDNA together with $\delta^2H_{C16:0\ Acid/Phytol}$ values and phytol:sterol ratios would reveal not only past cyanobacterial abundance, but also their abundance relative to eukaryotic algae.

Moreover, due to their good preservation, sedimentary $\delta^2H_{C16:0\ Acid/Phytol}$ values and phytol:sterol ratios, might be an alternative approach to reconstruct past cyanobacterial dynamics over geologic times when including degradation products of phytol (e.g., pristane, isomeric pristenes, phytadienes, phytenic acid and phytenes; Jeng *et al.,* 1997; Grossi *et al*., 1998; Rontani *et al*., 1999; Rontani & Volkman 2003) and sterols (stanols; Killops & Killops 2004; Brocks *et al.,* 2017; Brocks *et al.,* 2023). For instance, several paleoecological studies have already used the abundance of fossilized sterol degradation products in the geologic record as proxy for the increase of eukaryotic algae in the Cryogenian period > 600 million years ago (Brocks *et al.,* 2017; Brocks *et al.,* 2023). To minimize the impact of species variability in sterol content among eukaryotic algal species (Martin-Creuzburg & Merkel 2016; Volkman 2003; Rampen *et al.,* 2010; Taipale *et al.,* 2016), we propose phytol:sterol ratios of > 0.75 as an indicator of cyanobacterial dominance, representing values recorded in Rotsee during cyanobacterial blooms (Fig. 6B). Moreover, to increase the robustness of phytol:sterol ratios, we suggest excluding sterols potentially produced by sedimentary fungi, e.g., ergosterol or fungisterol (Weete 1989; Gessner & Chauvet 1993; Volkman 2003).

5. Conclusions

Biweekly measurements of algal lipid distributions and $\delta^2H_{C16:0\ Acid/Phytol}$, $\delta^2H_{C16:0\ Acid/Sterol}$, and $\delta^2H_{Sterol/Phytol}$ values in the water column of Rotsee were related to phytoplankton community composition over a one-year sampling period.

The summed biovolume of diatoms and golden algae was significantly positively correlated with $\delta^2H_{Sterol/Phytol}$ values and negatively correlated with $\delta^2H_{C16:0\ Acid/Sterol}$ values, while the remaining eukaryotic algal groups had the opposite relationships. Comparing measured $\delta^2H_{Lipid1/Lipid2}$ values with modeled $\delta^2H_{Lipid1/Lipid2}$ values incorporating multiple lipid

end-members indicated that algal mixotrophy and lake mixing may affect $\delta^2H_{Lipid1/Lipid2}$ values on a weekly scale, but that annual $\delta^2H_{Lipid1/Lipid2}$ values in the water column of eutrophic lake systems generally reflect the phytoplankton community composition. The analysis of algal lipid distributions indicated increasing concentrations of phytol and unsaturated C18 fatty acid during cyanobacterial blooms, and phytol:sterol ratios and C18:C16 ratios were significantly positively correlated with cyanobacterial biovolume. Due to the good preservation of lipids in sediment, particularly phytol:sterol ratios, combined with $\delta^2H_{C16:0\ Acid/Phytol}$ values, provide a promising tool for the reconstruction of past cyanobacterial blooms.

Generally, the interpretation of sedimentary $\delta^2H_{Lipid1/Lipid2}$ values and lipid ratios should consider the trophic status of the lacustrine system. In eutrophic lakes like Rotsee, phytoplankton are the main lipid source, likely overwhelming the isotopic imprint and lipid contribution of other autochthonous origins to the sediment. In oligotrophic lake systems and during periods of declining phytoplankton abundance, however, the relative importance of other aquatic lipid producers as well as allochthonous lipid sources might be higher, and $\delta^2H_{Lipid1/Lipid2}$ values could be further impacted by a higher proportion of phytoplankton mixotrophy. We therefore emphasize the interpretation of sedimentary $\delta^2H_{Lipid1/Lipid2}$ values and lipid ratios in a multi-proxy context integrating complementary lines of evidence.

Acknowledgements

This research was funded by a Swiss National Science Foundation (SNSF) Eccellenza Fellowship to SNL (PCEFP2 194211), an SNSF Prima Fellowship to CDJ (179783), and Eawag internal funds. Patrick Kathriner, Karin Beck, Nina Studhalter, Sandra Schmid, and Alois Zwyssig assisted with the field work. Argton Zeqiri and Serge Robert assisted with lipid extractions and alcohol analyses. Patrick Kathriner assisted with the preparation of water samples for nutrient analyses. Nitrogen and phosphorus concentrations were measured at the Eawag AuA laboratory.

Supplementary Material

A bathymetric map of Rotsee with the sampling area of biomass samples (Fig. S1) along with oxygen and temperature profiles throughout the water column during the different seasons (Fig. S2) are included in the supplement. Moreover, the relationship between peak dimensions and δ^2H values of cholesterol acetate and stigmasterol acetate standards (Fig. S3) and δ^2H values of brassicasterol, ergosterol, sitosterol, and stigmasterol (Fig. S6) are included. Modeled distributions of $\alpha^2_{C16:0\ Acid/Water}$ values, $\alpha^2_{Sterol/Water}$ values, and $\alpha^2_{Phytol/Water}$ values based on batch cultures of different phytoplankton groups (Ladd et al., 2025; Pilecky et al., 2024) are shown (Fig. S4), as well as the distribution of $\delta^2H_{C16:0\ Acid}$ values of seston and zooplankton based on field data (Pilecky et al., 2022) (Fig. S5). Additionally, correlation matrices indicating Spearman's correlations between $\delta^2H_{Lipid1/Lipid2}$ values and the relative biovolume of individual phytoplankton groups (Fig. S7, Fig. S8) are listed. Absolute concentrations of alcohols (Fig. S9) and fatty acids (Fig. S10) in the lake water column are shown as well as the NMDS plot of relative alcohol (Fig. S11A) and fatty acid (Fig. S11B) concentrations. Additionally, temperature and total phosphorus concentrations in the water column (Fig. S12), as well as an RDA plot indicating the relationships between relative phytoplankton biovolume and environmental variables (Fig. S13) are included.

Author contributions

Antonia Klatt: Conceptualization, Formal analysis, Investigation, Methodology, Visualization, Writing – original draft, Writing, review and editing. **Cindy De Jonge:** Funding acquisition, Investigation, Project administration, Writing – review and editing. **Daniel B. Nelson:** Conceptualization, Investigation, Methodology, Writing – review and editing. **Marta Reyes:** Investigation, Methodology, Writing – review and editing. **Carsten J. Schubert:** Conceptualization, Funding acquisition, Project administration, Resources, Writing – review and editing. **Nathalie Dubois:** Conceptualization, Project administration, Writing – review and editing. **S. Nemiah Ladd:** Conceptualization, Funding acquisition, Investigation, Methodology, Project administration, Supervision, Writing – review and editing.

Data availability

All data are available through the Dryad Digital Repository (https://doi.org/10.5061/dryad.9s4mw6mrm). All R scripts and related data files are uploaded in GitHub (https://github.com/antoniaKlatt/Klatt_etal_2025_phytoplankton_Rotsee).

References

Acevedo-Trejos, E., Brandt, G., Bruggeman, J., Merico, A., 2015: Mechanisms shaping size structure and functional diversity of phytoplankton communities in the ocean. Sci. Rep. 5, 8918.

Arhonditsis, G.B., Stow, C.A., Steinberg, L.J., Kenney, M.A., Lathrop, R.C., McBride, S.J., Reckhow, K.H., 2006: Exploring ecological patterns with structural equation modeling and Bayesian analysis. Ecol. Modell. 192, 385–409.

Baan, J., Holloway-Phillips, M., Nelson, D.B., Kahmen, A., 2023: The metabolic sensitivity of hydrogen isotope fractionation differs between plant compounds. Phytochem. 207, 113563.

Bauersachs, T., Talbot, H.M., Sidgwick, F., Sivonen, K., Schwark, L., 2017: Lipid biomarker signatures as tracers for harmful cyanobacterial blooms in the Baltic Sea. PLoS ONE 12, e0186360.

Bechtel, A., Schubert, C.J., 2009a: Biogeochemistry of particulate organic matter from lakes of different trophic levels in Switzerland. Org. Geochem. 40, 441–454.

Bechtel, A., Schubert, C. J., 2009b: A biogeochemical study of sediments from the eutrophic Lake Lugano and the oligotrophic Lake Brienz, Switzerland. Org. Geochem. 40, 1100-1114.

Biddanda, B., Ogdahl, M., Cotner, J., 2001: Dominance of bacterial metabolism in oligotrophic relative to eutrophic waters. L&O 3, doi: 10.4319/lo.2001.46.3.0730.

Bloesch, J., 1974: Sedimentation und Phosphorhaushalt im Vierwaldstättersee (Horwer Bucht) und im Rotsee. Schweiz. Z. Hydrologie 36, 71–186.

Bodelier, P.L.E., Bär Gillisen, M.-J., Hordijk, K., Sinninghe Damsté, J.S., Rijpstra, W.I.C., Geenevasen, J.A.J., Dunfield, P.F., 2009: A reanalysis of phospholipid fatty acids as ecological biomarkers for methanotrophic bacteria. *The ISME Journal* 3, 606–617.

Brocks, J.J., Nettersheim, B.J., Adam, P., Schaeffer, P., Jarrett, A.J.M., Güneli, N., Liyanage, T., van Maldegem, L. M., Hallmann, C., Hope, J.M., 2023: Lost world of complex life and the late rise of the eukaryotic crown. Nature 618, 767–773.

Brocks, J.J., Jarrett, A.J.M., Sirantoine, E., Hallmann, C., Hoshino, Y., Liyanage, T., 2017: The rise of algae in Cryogenian oceans and the emergence of animals. Nature 548, 578–581.

Calderini, M.L., Pääkkönen, S., Salmi, P., Peltomaa, E., Taipale, S.J., 2023: Temperature, phosphorus and species composition will all influence phytoplankton production and content of polyunsaturated fatty acids. J. Plankton Res. 45, 625–635.

Callieri, C., Caravati, E., Morabito, G., Oggioni, A., 2006: The unicellular freshwater cyanobacterium *Synechococcus* and mixotrophic flagellates: evidence for a functional association in an oligotrophic, subalpine lake. Freshw. Biol. 51, 263–273.

Callisto, M., Molozzi, J., Barbosa, J.L.E., 2014: Eutrophication of Lakes, in: Ansari, A., Gill, S. (Eds.), Eutrophication: Causes, Consequences and Control. Springer, Dordrecht, pp. 55–71.

Cao, X., Xu, X., Bian, R., Wang, Y., Yu, H., Xu, Y. Duan, G., Bi, L., Chen, P., Gao, S., Wang, J., Peng, J., Qu, J., 2020: Sedimentary ancient DNA metabarcoding delineates the contrastingly temporal change of lake cyanobacterial communities. Water Res. 183, 116077.

Capo, E., Debroas, D., Arnaud, F., Domaizon, I., 2015: Is Planktonic Diversity Well Recorded in Sedimentary DNA? Toward the Reconstruction of Past Protistan Diversity. Microb. Ecol. 70, 865–875.

Capo, E., Monchamp, M.-E., Coolen, M.J.L., Domaizon, I., Armbrecht, L., Bertilsson, S., 2022: Environmental paleomicrobiology: using DNA preserved in aquatic sediments to its full potential. Environ. Microbiol. 24, 2201–2209.

Caron, D.A., Sanders, R.W., Lim, E.L., Marrasé, C., Amaral, L.A., Whitney, S., Aoki, R.B., Porters, K.G., 1993: Light-dependent phagotrophy in the freshwater mixotrophic chrysophyte *Dinobryon cylindricum*. Microb. Ecol. 25, 93–111.

Cormier, M.-A., Berard, J.-B., Bougaran, G., Trueman, C.N., Mayor, D.J., Lampitt, R.S., Kruger, N.J., Flynn, K.J., Rickaby, R.E.M., 2022: Deuterium in marine organic biomarkers: toward a new tool for quantifying aquatic mixotrophy. New Phytol. 234, 776–782.

Cormier, M.-A., Werner, R.A., Sauer, P.E., Gröcke, D.R., Leuenberger, M.C., Wieloch, T., Schleucher, J., Kahmen, A., 2018: ^{2}H-fractionations during the biosynthesis of carbohydrates and lipids imprint a metabolic signal on the δ^{2}H values of plant organic compounds. New Phytol. 218, 479–491.

Coveney, M.F., Cronberg, G., Enell, M., Larsson, K., Olofsson, L., 1977: Phytoplankton, Zooplankton and Bacteria: Standing Crop and Production Relationships in a Eutrophic Lake. Oikos 29, 5–21.

Cvetkoska, A., Jovanovska, E., Hauffe, T., Donders, T.H., Levkov, Z., van de Waal, D.B., Reed, J.M., Francke, A., Vogel, H., Wilke, T., Wagner, B., Wagner-Cremer, F., 2021: Drivers of phytoplankton community structure change with ecosystem ontogeny during the Quaternary. Quat. Sci. Rev. 265, 107046.

Dale, B., Fjellså, A., 1994: Dinoflagellate Cysts as Paleoproductivity Indicators: State of the Art, Potential, and Limits, in: Zahn, R., Pedersen, T.F., Kaminski, M.A., Labeyrie, L. (Eds.), Carbon Cycling in the Glacial Ocean: Constraints on the Ocean's Role in Global Change. NATO ASI Series 17. Springer, Berlin, Heidelberg, pp. 521–537.

Darling, W.G., Bath, A.H., Gibson, J.J., Kazimierz, R., 2006: Isotopes in water. in: Leng, M.J. (Eds.), Isotopes in Palaeoenvironmental Research. Springer, Dordrecht, pp. 1–66.

Desmond, E., Gribaldo, S., 2009: Phylogenomics of Sterol Synthesis: Insights into the Origin, Evolution, and Diversity of a Key Eukaryotic Feature. Genome Biol. Evol. 1, 364–381.

1001 Dufourc, E.J., 2008: Sterols and membrane dynamics. J. Chem. Biol. 1, 63–77.

1002 Fiskal, A., Deng, L., Michel, A., Eickenbusch, P., Han, X., Lagostina, L., Zhu, R., Sander, M.,
1003 Schroth, M.H., Bernasconi, S.M., Dubois, N., Lever, M.A., 2019: Effects of eutrophication
1004 on sedimentary organic carbon cycling in five temperate lakes. Biogeosci. 16, 3725–
1005 3746.

1006 Gessner, M.O., Chauvet, E., 1993: Ergosterol-to-Biomass Conversion Factors for Aquatic
1007 Hyphomycetes. Appl. Environ. Microbiol. 59, 502–507.

1008 Goad, L.J., 1981: Sterol biosynthesis and metabolism in marine invertebrates. Pure
1009 Appl. Chem. 51, 837–852.

1010 Gray, J.R., Lacrampe-Couloume, G., Gandhi, D., Scow, K.M., Wilson, R.D., Mackay, D.M.,
1011 Sherwood Lollar, B., 2002: Carbon and Hydrogen Isotopic Fractionation during
1012 Biodegradation of Methyl tert-Butyl Ether. Environ. Sci. Tech. 36, 1931–1938.

1013 Grossi, V., Hirschler, A., Raphel, D., Rontani, J.-F., Leeuw, J.W. de, Bertrand, J.-C., 1998:
1014 Biotransformation pathways of phytol in recent anoxic sediments. Org. Geochem. 29,
1015 845–861.

1016 Han, X., Schubert, C.J., Fiskal, A., Dubois, N., Lever, M.A., 2020: Eutrophication as a driver
1017 of microbial community structure in lake sediments. Environ. Microbiol. 22, 3446-3462.
1018
1019 Harrell Jr. F., 2023: Hmisc: Harrell Miscellaneous. R package version 5.1-0.

1020 Harvey. H.R., Fallon, R.D., Patton, J.S., 1986: The effect of organic matter and oxygen on
1021 the degradation of bacterial membrane lipids in marine sediments. Geochim.
1022 Cosmochim. Acta 50, 795–804.

1023 Hastie, T., Tibshirani, R., Friedman, J., 2009: The Elements of Statistical Learning, second
1024 ed., Springer, New York.

1025 Heinzelmann, S.M., Chivall, D., M'Boule, D., Sinke-Schoen, D., Villanueva, L., Sinninghe
1026 Damsté, J.S., Schouten, S., van der Meer, M.T.J., 2015a: Comparison of the effect of
1027 salinity on the D/H ratio of fatty acids of heterotrophic and photoautotrophic
1028 microorganisms. FEMS Microbiol. Lett. 362, fnv065.

1029 Heinzelmann, S.M., Villanueva, L., Sinke-Schoen, D., Sinninghe Damsté, J.S., Schouten, S.,
1030 van der Meer, M.T.J., 2015b: Impact of metabolism and growth phase on the
1031 hydrogen isotopic composition of microbial fatty acids. Front. Microbiol. 6, 408.

1032 Heinzelmann, S.M., Villanueva, L., Lipsewers, Y.A., Sinke-Schoen, D., Sinninghe Damsté,
1033 J.S., Schouten, S., van der Meer, M.T.J., 2018: Assessing the metabolism of
1034 sedimentary microbial communities using the hydrogen isotopic composition of fatty
1035 acids. Org. Geochem.124, 123–132.

1036 Henson, S.A., Cael, B.B., Allen, S.R., Dutkiewicz, S., 2021: Future phytoplankton diversity in
1037 a changing climate. Nat. Commun. 12, 5372.

1038 Hinder, S.L., Hays, G.C., Edwards, M., Roberts, E.C., Walne, A.W., Gravenor, M.B., 2012:
1039 Changes in marine dinoflagellate and diatom abundance under climate change.
1040 Nat. Clim. Change 2, 271–275.

1041 Hirave, P., Glendell, M., Birkholz, A., Alewell, C., 2021: Compound-specific isotope analysis
1042 with nested sampling approach detects spatial and temporal variability in the sources
1043 of suspended sediments in a Scottish mesoscale catchment. Sci. Total Environ. 755,
1044 142916.

1045 Hollander, D. J., McKenzie, J. A.; ten Haven, H. L., 1992: A 200 year sedimentary record of
1046 progressive eutrophication in lake Greifen (Switzerland): Implications for the origin of
1047 organic-carbon-rich sediments. Geology 20, 825–828.

Holloway-Phillips, M., Cernusak, L.A., Nelson, D.B., Lehmann, M.M., Tcherkez, G., Kahmen, A., 2023: Covariation between oxygen and hydrogen stable isotopes declines along the path from xylem water to wood cellulose across an aridity gradient. New Phytol. 240, 1758–1773.

Huang, Y., Shuman, B., Wang, Y., Webb, T., 2004: Hydrogen isotope ratios of individual lipids in lake sediments as novel tracers of climatic and environmental change: a surface sediment test. J. Paleolimnol. 31, 363–375.

Huisman, J., Codd, G.A., Paerl, H.W., Ibelings, B.W., Verspagen, J.M.H., Visser, P.M., 2018: Cyanobacterial blooms. Nat. Rev. Microbiol. 16, 471–483.

Irish, A.E., 1979: *Gymnodinium helveticum* Penard F. *Achroum* Skuja a case of phagotrophy. *Brit. Phycol. J*. 14, 11–15.

Jankowiak, J., Hattenrath-Lehmann, T., Kramer, B.J., Ladds, M., Gobler, C.J., 2019: Deciphering the effects of nitrogen, phosphorus, and temperature on cyanobacterial bloom intensification, diversity, and toxicity in western Lake Erie. L&O 64, 1347–1370.

Jeng, W.-L., Huh, C.-A., Chen, C.-L., 1997: Alkanol and sterol degradation in a sediment core from the continental slope off southwestern Taiwan. Chemosphere 35, 2515–2523.

Jiang, M., Nakano, S.-I., 2022: The crucial influence of trophic status on the relative requirement of nitrogen to phosphorus for phytoplankton growth. Water Res. 222, 118868.

Kaneda, T., 1991: Iso- and anteiso-fatty acids in bacteria: biosynthesis, function, and taxonomic significance. Microbiol. Rev. 55, 288–302.

Kassambara, A., 2023: ggcorrplot: Visualization of a Correlation Matrix using 'ggplot2'. R package version 0.1.4.1.

Kawamura, K., Ishiwatari, R., Ogura, K., 1987: Early diagenesis of organic matter in the water column and sediments: Microbial degradation and resynthesis of lipids in Lake Haruna. Org. Geochem. 11, 251–264.

Killops, S., Killops, V., 2004: Chemical Stratigraphic Concepts and Tools. in: Introduction to Organic Geochemistry. Blackwell publishing company, Oxford, pp. 166-245.

Kohler, H.-P., Åhring, B., Albella, C., Ingvorsen, K., Keweloh, H., Laczkó, E., Stupperich, E., Tomei, F., 1984: Bacteriological studies on the sulfur cycle in the anaerobic part of the hypolimnion and in the surface sediments of Rotsee in Switzerland. FEMS Microbiology Letters 21, 279–286.

Kopp, R. E., Kirschvink, J. L., Hilburn, I. A., Nash, C. Z., 2005: The Paleoproterozoic snowball Earth: A climate disaster triggered by the evolution of oxygenic photosynthesis. PNAS 102, 11131–11136.

Ladd, S.N., Dubois, N., Schubert, C.J., 2017: Interplay of community dynamics, temperature, and productivity on the hydrogen isotope signatures of lipid biomarkers. Biogeosci. 14, 3979–3994.

Ladd, S.N., Nelson, D.B., Schubert, C.J., Dubois, N., 2018: Lipid compound classes display diverging hydrogen isotope responses in lakes along a nutrient gradient. Geochim. Cosmochim. Acta 237, 103–119.

Ladd, S.N., Nelson, D.B., Matthews, B., Dyer, S., Limberger, R., Klatt, A., Narwani, A., Dubois, N., Schubert, C.J., 2025: Taxon-specific hydrogen isotope signals in cultures and mesocosms facilitate ecosystem and hydroclimate reconstruction.Geochim. Cosmochim. Acta 390, 199–210.

Lammers, J.M., Schubert, C.J., Middelburg, J.J., Reichart, G.J., 2016: Carbon flows in eutrophic Lake Rotsee: a ^{13}C-labelling experiment. Biogeochemistry 131, 147–162.

Lang, I., Hodac, L., Friedl, T., Feussner, I., 2011: Fatty acid profiles and their distribution patterns in microalgae: a comprehensive analysis of more than 2000 strains from the SAG culture collection. BMC Plant Biol 11, 124.

Leavitt, P.R., 1993: A review of factors that regulate carotenoid and chlorophyll deposition and fossil pigment abundance. J. Paleolimnol. 9, 109–127.

Li, Y., Wu, S., Wang, L., Li, Y., Shi, F., Wang, X., 2010: Differentiation of bacteria using fatty acid profiles from gas chromatography–tandem mass spectrometry. J. Sci. Food Agric. 90, 1380–1383.

Liang, Z., Soranno, P.A., Wagner, T., 2020: The role of phosphorus and nitrogen on chlorophyll a: Evidence from hundreds of lakes. Water Res.185, 116236.

Lin, Q., Zhang, K., McGowan, S., Capo, E., Shen, J., 2021: Synergistic impacts of nutrient enrichment and climate change on long-term water quality and ecological dynamics in contrasting shallow-lake zones. L&O 66, 3271–3286.

Litchman, E., de Tezanos Pinto, P., Edwards, K.F., Klausmeier, C.A., Kremer, C., T., Thomas, M.K., 2015: Global biogeochemical impacts of phytoplankton: a trait-based perspective. J. Ecol. 103, 1384–1396.

Liu, M., Huang, Y., Hu, J., He, J., Xiao, X., 2023: Algal community structure prediction by machine learning. Environ. Sci. Ecotechnol. 14, 100233.

Lotter, A.F., 1998: The recent eutrophication of Baldeggersee Switzerland as assessed by fossil diatom assemblages. The Holocene 8, 395–405.

Lotter, A.F., 1989: Subfossil and modern diatom plankton and the paleolimnology of Rotsee Switzerland since 1850. Schweiz. Z. Hydrologie 51, 338–350.

M'Boule, D., Chivall, D., Sinke-Schoen, D., Sinninghe Damsté, J.S., Schouten, S., van der Meer, M.T.J., 2014: Salinity dependent hydrogen isotope fractionation in alkenones produced by coastal and open ocean haptophyte algae. Geochim. Cosmochim. Acta 130, 126–135.

Mancini, S.A., Ulrich, A.C., Lacrampe-Couloume, G., Sleep, B., Edwards, E.A., Sherwood Lollar, B., 2003: Carbon and Hydrogen Isotopic Fractionation during Anaerobic Biodegradation of Benzene. Appl. Environ. Microbiol. 69, 191–198.

Martin-Creuzburg, D., von Elert, E., 2004: Impact of 10 Dietary Sterols on Growth and Reproduction of *Daphnia galeata*. J. Chem. Ecol. 30, 483–500.

Martin-Creuzburg, D., von Elert, E., Hoffmann, K.H., 2008: Nutritional constraints at the cyanobacteria—*Daphnia magna* interface: The role of sterols. L&O 53, 456–468.

Martin-Creuzburg, D., Merkel, P., 2016: Sterols of freshwater microalgae: potential implications for zooplankton nutrition. J. Plankton Res. 38, 865–877.

Matsui, H., Shiozaki, K., Okumura, Y., Ishikawa, M., Waqalevu, V., Hayasaka, O., Honda, A., Kotani, T., 2020: Effects of phosphorus deficiency of a microalga *Nannochloropsis oculata* on its fatty acid profiles and intracellular structure and the effectiveness in rotifer nutrition. Algal Res. 49, 101905.

Mattern, J.P., Glauninger, K., Britten, G.L., Casey, J.R., Hyun, S., Wu, Z., Armbrust, E.V., Harchaoui, Z., Ribalet, F., 2022: A Bayesian approach to modeling phytoplankton population dynamics from size distribution time series. PLoS Comput. Biol. 18, e1009733.

Mayr, M.J., Zimmermann, M., Dey, J., Brand, A., Wehrli, B., Bürgmann, H., 2020: Growth and rapid succession of methanotrophs effectively limit methane release during lake overturn. Commun. Biol. 3, 108.

McGowan, S., Barker, P., Haworth, E.Y., Leavitt, P.R., Maberly, S.C., Pates, J., 2012: Humans and climate as drivers of algal community change in Windermere since 1850. Freshw. Biol. 57, 260–277.

Meyers, P.A., Ishiwatari, R., 1993: Lacustrine organic geochemistry—an overview of indicators of organic matter sources and diagenesis in lake sediments. Org. Geochem. 20, 867-900.

Miljević, N., Golobočanin, D., 2007: Potential Use of Environmental Isotopes in Pollutant Migration Studies. Arh. Hig. Rada. Toksikol. 58, 251–262.

Mouradian, M., Panetta, R.J., de Vernal, A., Gélinas, Y., 2007: Dinosterols or dinocysts to estimate dinoflagellate contributions to marine sedimentary organic matter? L&O 52, 2569–2581.

Muñoz-Marín, M.D.C., López-Lozano, A., Moreno-Cabezuelo, J.Á., Díez, J., García-Fernández, J.M., 2024: Mixotrophy in cyanobacteria. Curr. Opin. Microbiol. 78, 102432.

Naeher, S., Smittenberg, R.H., Gilli, A., Kirilova, E.P., Lotter, A.F., Schubert, C.J., 2012: Impact of recent lake eutrophication on microbial community changes as revealed by high resolution lipid biomarkers in Rotsee (Switzerland). Org. Geochem. 49, 86–95.

Narwani, A., Reyes, M., Pereira, A.L., Penson, H., Dennis, S.R., Derrer, S., Spaak, P., Matthews, B., 2019: Interactive effects of foundation species on ecosystem functioning and stability in response to disturbance. Proc R Soc B*:* Biol. Sci. 286, 20191857.

Naselli-Flores, L., Padisák, J., 2023: Ecosystem services provided by marine and freshwater phytoplankton. Hydrobiologia 850, 2691–2706.

Nelson, D.B., Sachs, J.P., 2014: The influence of salinity on D/H fractionation in dinosterol and brassicasterol from globally distributed saline and hypersaline lakes. Geochim. Cosmochim. Acta 133, 325–339.

Newberry, S.L., Nelson, D.B., Kahmen, A., 2017: Cryogenic vacuum artifacts do not affect plant water-uptake studies using stable isotope analysis. Ecohydrology 10, e1892.

Not, F., Siano, R., Kooistra, W.H.C.F., Simon, N., Vaulot, D., Probert, I., 2012: Diversity and Ecology of Eukaryotic Marine Phytoplankton. Adv. Bot. Res. 64, 1–53.

Nwosu, E.C., Brauer, A., Monchamp, ME., Pinkerneil, S., Bartholomäus, A., Theuerkauf, M., Schmidt, J.-P., Stoof-Leichsenring, K.R., Wietelmann, T., Kaiser, J., Wagner, D., Liebner, S., 2023: Early human impact on lake cyanobacteria revealed by a Holocene record of sedimentary ancient DNA. Commun Biol 6, 72.

Oksanen, J., Simpson, G,., Blanchet, F., Kindt, R., Legendre, P., Minchin, P., O'Hara, R.B., Solymos, P., Stevens, M.H.H., Szoecs, E., Wagner, H., Barbour, M., Bedward, M., Bolker, B., Borcard, D., Carvalho, G., Chirico, M., De Caceres, M., Durand, S., Evangelista, H.B.A., FitzJohn, R., Friendly, M., Furneaux, B., Hannigan, G., Hill, M.O., Lahti, L., McGlinn, D., Ouellette, M.-H., Cunha, E.R., Smith, T., Stier, A., Ter Braak, C.J.F., Weedon, J., 2022: vegan: Community Ecology Package. R package version 2.6-4.

Osman, M.B., Tierney, J.E., Zhu, J., Tardif, R., Hakim, G.J., King, J., Poulsen, C.J., 2021: Globally resolved surface temperatures since the Last Glacial Maximum. Nature 599, 239–244.

Pal, S., Gregory-Eaves, I., Pick, F.R., 2015: Temporal trends in cyanobacteria revealed through DNA and pigment analyses of temperate lake sediment cores. J. Paleolimnol. 54, 87–101.

1189 Pålsson, C., Granéli, W., 2004: Nutrient limitation of autotrophic and mixotrophic
1190 phytoplankton in a temperate and tropical humic lake gradient. J. Plankton Res. 26,
1191 1005–1014.

1192 Peltomaa, E., Asikainen, H., Blomster, J., Pakkanen, H., Rigaud, C., Salmi, P., S. Taipale,
1193 S., 2023: Phytoplankton group identification with chemotaxonomic biomarkers: In
1194 combination they do better. Phytochem. 209, 113624.

1195 Peltomaa, E. T., Aalto, S. L., Vuorio, K. M., Taipale, S. J. 2017: The Importance of
1196 Phytoplankton Biomolecule Availability for Secondary Production. Front. ecol. evol. 5,
1197 128.

1198 Perdue, E.M., Koprivnjak, J.-F., 2007: Using the C/N ratio to estimate terrigenous inputs of
1199 organic matter to aquatic environments. Estuar. Coast. Shelf Sci. 73, 65–72.

1200 Piepho, M., Martin-Creuzburg, D., Wacker, A., 2010: Simultaneous effects of light intensity
1201 and phosphorus supply on the sterol content of phytoplankton. PLoS ONE 5, e15828.

1202 Piepho, M., Martin-Creuzburg, D., Wacker, A., 2012: Phytoplankton sterol contents vary with
1203 temperature, phosphorus and silicate supply: a study on three freshwater species.
1204 Eur. J. Phycol. 47, 138–145.

1205 Piironen, V., Lindsay, D.G., Miettinen, T.A., Toivo, J., Lampi, A.-M., 2000: Plant sterols:
1206 biosynthesis, biological function and their importance to human nutrition. J. Sci. Food
1207 Agric. 80, 939–966.

1208 Pilecky, M., Kainz, M.J., Wassenaar, L.I., 2024: Exploring hydrogen isotope fractionation in
1209 lipid biomolecules of freshwater algae: implications for ecological and paleoenvironmental
1210 studies. IEHS 60, 585–595.

1211 Pilecky, M., Kämmer, S.K., Mathieu-Resuge, M., Wassenaar, L.I., Taipale, S.J., Martin-
1212 Creuzburg, D., Kainz, M.J., 2022: Hydrogen isotopes (δ^2H) of polyunsaturated fatty
1213 acids track bioconversion by zooplankton. Funct. Ecol. 36, 538–549.

1214 Podani, J., Miklós, I., 2002: Resemblance coefficients and the horseshoe effect in principal
1215 coordinates analysis. Ecology, 83: 3331-3343.

1216 Ptacnik, R., Solimini, A.G., Andersen, T., Tamminen, T., Brettum, P., Lepistö, L., Willén, E.,
1217 Rekolainen, S., 2008: Diversity predicts stability and resource use efficiency in natural
1218 phytoplankton communities. PNAS 105, 5134–5138.

1219 R Core Team, 2023: R: A Language and Environment for Statistical Computing. Vienna,
1220 Austria: R Foundation for Statistical Computing.

1221 Rampen, S.W., Abbas, B.A., Schouten, S., Sinninghe Damste, J.S., 2010: A comprehensive
1222 study of sterols in marine diatoms Bacillariophyta: Implications for their use as tracers
1223 for diatom productivity. L&O 55, 91–105.

1224 Reuss, N., Conley, D.J., Bianchi, T.S., 2005: Preservation conditions and the use of
1225 sediment pigments as a tool for recent ecological reconstruction in four Northern
1226 European estuaries. Mar. Chem. 95, 283–302.

1227 Revelle, W., 2024: psych: Procedures for Psychological, Psychometric, and Personality
1228 Research. R package version 2.4.3.

1229 Rontani, J.-F., Bonin, P.C., Volkman, J.K., 1999: Biodegradation of Free Phytol by Bacterial
1230 Communities Isolated from Marine Sediments under Aerobic and Denitrifying
1231 Conditions. Appl. Environ. Microbiol. 65, 5484–5492.

1232 Rontani, J.-F., Volkman, J.K., 2003: Phytol degradation products as biogeochemical tracers
1233 in aquatic environments. Org. Geochem. 34, 1–35.

1234 Rustan, A.C., Drevon, C.A., 2005: Fatty Acids: Structures and Properties, in: eLS. John
1235 Wiley and Sons, Chichester, UK.

1236 Saad, J.F., Unrein, F., Tribelli, P.M., López, N., Izaguirre, I., 2016: Influence of lake trophic
1237 conditions on the dominant mixotrophic algal assemblages. J. Plankton Res. 38,
1238 818–829.

1239 Sachs, J.P., Kawka, O.E., 2015: The Influence of Growth Rate on $^{2}H/^{1}H$ Fractionation in
1240 Continuous Cultures of the Coccolithophorid *Emiliania huxleyi* and the Diatom
1241 *Thalassiosira pseudonana*. PLoS ONE 10, e0141643.

1242 Sachs, J.P., Schwab, V.F., 2011: Hydrogen isotopes in dinosterol from the Chesapeake Bay
1243 estuary. Geochim. Cosmochim. Acta 75, 444–459.

1244 Sachse, D., Billault, I., Bowen, G.J., Chikaraishi, Y., Dawson, T.E., Feakins, S.J., Magill,
1245 C.R., McInerney, F.A., van der Meer, M.T.J., Polissar, P., Robins, R.J., Sachs, J.P.,
1246 Schmidt, H.-L., Sessions, A.L., White, J.W.C., West, J.B., Kahmen, A., 2012:
1247 Molecular Paleohydrology: Interpreting the Hydrogen-Isotopic Composition of Lipid
1248 Biomarkers from Photosynthesizing Organisms. Annu. Rev. Earth Planet. Sci. 40,
1249 221–249.

1250 Sauer, P.E., Eglinton, T.I., Hayes, J.M., Schimmelmann, A., Sessions, A.L., 2001:
1251 Compound-specific D/H ratios of lipid biomarkers from sediments as a proxy for
1252 environmental and climatic conditions. Geochim. Cosmochim. Acta 65, 213–222.

1253 Schimmelmann, A., Sessions, A.L., Mastalerz, M., 2006: Hydrogen isotopic D/H composition
1254 of organic matter during diagenesis and thermal maturation. Annu. Rev. Earth Planet.
1255 Sci. 34, 501–533.

1256 Schmidt, H.-L., Werner, R.A., Eisenreich, W., 2003: Systematics of ^{2}H patterns in natural
1257 compounds and its importance for the elucidation of biosynthetic pathways.
1258 Phytochem. Rev. 2, 61–85.

1259 Schouten, S., Ossebaar, J., Schreiber, K., Kienhuis, M.V.M., Langer, G., Benthien, A., Bijma,
1260 J., 2006: The effect of temperature, salinity and growth rate on the stable hydrogen
1261 isotopic composition of long chain alkenones produced by *Emiliania huxleyi* and
1262 *Gephyrocapsa oceanica*. Biogeosci. 3, 113–119.

1263 Schubert, C.J., Villanueva, J., Calvert, S.E., Cowie, G.L., von Rad, U., Schulz, H., Berner, U.,
1264 Erlenkeuser, H., 1998: Stable phytoplankton community structure in the Arabian Sea
1265 over the past 200,000 years. Nature 394, 563–566.

1266 Schwab, V.F., Garcin, Y., Sachse, D., Todou, G., Séné, O., Onana, J.-M., Achoundong, G.,
1267 Gleixner, G., 2015: Dinosterol δD values in stratified tropical lakes (Cameroon) are
1268 affected by eutrophication. Org. Geochem. 88, 35–49.

1269 Serrazanetti, G.P., Conte, L.S., Pagnucco, C., Bergami, C., Milani, L., 1992: Sterol content in
1270 zooplankton of Adriatic Sea open waters. *Comp. Biochem. Physiol.* 102, 743–746.

1271 Shen, J., Pearson, A., Henkes, G.A., Zhang, Y.G., Chen, K., Li, D. Wankel, S.D., Finney,
1272 S.C. Shen, Y., 2018: Improved efficiency of the biological pump as a trigger for the
1273 Late Ordovician glaciation. *Nat. Geosci.* 11, 510–514.

1274 Shimoda, Y., Azim, M.E., Perhar, G., Ramin, M., Kenney, M.A., Sadraddini, S., Gudimov, A.,
1275 Arhonditsis, G.B., 2011: Our current understanding of lake ecosystem response to
1276 climate change: What have we really learned from the north temperate deep lakes? J.
1277 Great Lakes Res. 37, 173–193.

1278 Simon, M., Cho, B.C., Azam, F., 1992: Significance of Bacterial Biomass in Lakes and the Ocean:
1279 Comparison to Phytoplankton Biomass and Biogeochemical
1280 Implications. Mar. Ecol. Prog. Ser. 86, 103–10.

1281 Smol, J.P., 1985: The ratio of diatom frustules to chrysophycean statospores: A useful
1282 paleolimnological index. Hydrobiologia 123, 199–208.

1283 Stivrins, N., Soininen, J., Amon, L., Fontana, S.L., Gryguc, G., Heikkilä, M., Heiri, O.,
1284 Kisielienė, D., Reitalu, T., Stančikaitė, M., Veski, S., Seppä, H., 2016: Biotic turnover
1285 rates during the Pleistocene-Holocene transition. Quat. Sci. Rev. 151, 100–110.

1286 Summons, R.E., Welander, P.V., Gold, D.A., 2022: Lipid biomarkers: molecular tools for
1287 illuminating the history of microbial life. Nat. Rev. Microbiol. 20, 174–185.

1288 Taipale, S.J., Strandberg, U., Peltomaa, E., Galloway, A.W.E., Ojala, A., Brett, M.T., 2013:
1289 Fatty acid composition as biomarkers of freshwater microalgae: analysis of 37 strains
1290 of microalgae in 22 genera and in seven classes. Aquat. Microb. Ecol. 71, 165–178.

1291 Taipale, S.J., Hiltunen, M., Vuorio, K., Peltomaa, E., 2016: Suitability of Phytosterols
1292 Alongside Fatty Acids as Chemotaxonomic Biomarkers for Phytoplankton.
1293 Front. Plant Sci. 7, 212.

1294 Thevenon, F., Adatte, T., Poté, J., Spangenberg, J. E., 2012: Recent human-induced trophic
1295 change in the large and deep perialpine Lake Lucerne (Switzerland) compared to
1296 historical geochemical variations. Palaeogeogr. Palaeoclimatol. Palaeoecol. 363-364,
1297 37–47.

1298 Thorpe, A.C., Mackay, E.B., Goodall, T., Bendle, J.A., Thackeray, S.J., Maberly, S.C., Read,
1299 D.S., 2024: Evaluating the use of lake sedimentary DNA in palaeolimnology: A
1300 comparison with long-term microscopy-based monitoring of the phytoplankton
1301 community. Mol. Ecol. Resour. 24, e13903.

1302 Torres-Romero, I., Zhang, H., Wijker, R.S., Clark, A.J., McLeod, R.E., Jaggi, M., Stoll, H.M.,
1303 2024: Hydrogen isotope fractionation is controlled by CO_2 in coccolithophore lipids.
1304 PNAS 121, e2318570121.

1305 von Utermöhl, H., 1931: Neue Wege in der quantitativen Erfassung des Planktons. Mit
1306 besonderer Berücksichtigung des Ultraplanktons. Verh. Int. Verein. Theor. Angew.
1307 Limnol., 567–596.

1308 Vander Zanden, H.B., Soto, D.X., Bowen, G.J., Hobson, K.A., 2016: Expanding the Isotopic
1309 Toolbox: Applications of Hydrogen and Oxygen Stable Isotope Ratios to Food Web
1310 Studies. Front. ecol. evol. 4, 20.

1311 Vimeux, F., Masson, V., Jouzel, J., Stievenard, M., Petit, J.R., 1999: Glacial–interglacial
1312 changes in ocean surface conditions in the Southern Hemisphere. Nature 398, 410–
1313 413.

1314 Vogler, P., 1965: Beiträge zur Phosphatanalytik in der Limnologie. Die Bestimmung des
1315 gelösten Orthophosphates. Fortschr. Wasserchem. Grenzgeb. 2, 109–119.

1316 Volkman, J.K., 2003: Sterols in microorganisms. *Appl. Microbiol. Biotechnol.* 60, 495–506.

1317 Wacker, A., Martin-Creuzburg, D., 2012: Biochemical nutrient requirements of the rotifer
1318 *Brachionus calyciflorus*: co-limitation by sterols and amino acids. Funct. Ecol. 26,
1319 1135–1143.

1320 Weete, J.D., 1989: Structure and Function of Sterols in Fungi. Adv. Lipid Res. 23, 115–167.

1321 Wei, J.H., Yin, X., Welander, P.V., 2016: Sterol Synthesis in Diverse Bacteria.
1322 Front. microbiol. 7, 990.

1323 Wickham, H., 2009: ggplot2: Elegant Graphics for Data Analysis, second ed. Springer, New
1324 York.

1325 Wilke, C., 2020: cowplot: Streamlined Plot Theme and Plot Annotations for 'ggplot2'. R
1326 package version 1.1.1.

1327 Wille, E., Hoffmann, L., 1991: Population dynamics of the dinoflagellate *Gymnodinium*
1328 *helveticum* Penard in the reservoir of Esch-sur-Sûre G.-D. of Luxembourg. Belg. J.
1329 Bot. 124, 109–114.

Witkowski, C.R., van der Meer, M.T.J., Blais, B., Sinninghe Damsté, J.S., Schouten, S., 2020: Algal biomarkers as a proxy for pCO_2: Constraints from late quaternary sapropels in the eastern Mediterranean. Org. Geochem. 150, 104123.

Wittenborn, A.K., Schmale, O., Thiel, V., 2020: Zooplankton impact on lipid biomarkers in water column vs. surface sediments of the stratified Eastern Gotland Basin Central Baltic Sea. PLoS ONE 15, e0234110.

Wobus, A., Bleul, C., Maassen, S., Scheerer, C., Schuppler, M., Jacobs, E., IRöske, I., 2003: Microbial diversity and functional characterization of sediments from reservoirs of different trophic state. FEMS Microbiol. Ecol. 46, 331–347.

Yuan, L.L., Pollard, A.I., 2018: Changes in the relationship between zooplankton and phytoplankton biomasses across a eutrophication gradient. L&O 63, 2493–2507.

Yuan, Z., Liu, D., Masqué, P., Zhao, M., Song, X., Keesing, J.K., 2020: Phytoplankton Responses to Climate-Induced Warming and Interdecadal Oscillation in North-Western Australia. Paleoceanogr. Paleoclimatol. 35, e2019PA003712.

Zagarese, H.E., Sagrario, M.D.L.Á.G., Wolf-Gladrow, D., Nõges, P., Nõges, T., Kangur, K., Matsuzaki, S.-I.S., Kohzu, A., Vanni, M.J., Özkundakci, D., Echaniz, S.A., Vignatti, A., Grosman, F., Sanzano, P., Van Dam, B., Knoll, L.B., 2021: Patterns of CO_2 concentration and inorganic carbon limitation of phytoplankton biomass in agriculturally eutrophic lakes. Water Res. 190, 116715.

Zeman-Kuhnert, S., Heim, C., Öztoprak, M., Thiel, V., 2023: Reconstructing eutrophication trends of a shallow lake environment using biomarker dynamics and sedimentary sterols. Org. Geochem. 177, S. 104555.

Zhang, X., Gillespie, A.L., Sessions, A.L., 2009: Large D/H variations in bacterial lipids reflect central metabolic pathways. PNAS 106, 12580–12586.

Zhang, Z., Sachs, J.P., 2007: Hydrogen isotope fractionation in freshwater algae: I. Variations among lipids and species. Org. Geochem. 38, 582–608.

Zhang, Z., Sachs, J.P., Marchetti, A., 2009: Hydrogen isotope fractionation in freshwater and marine algae: II. Temperature and nitrogen limited growth rate effects. Org. Geochem. 40, 428–439.

Supplementary Material for: Algal lipid distributions and hydrogen isotope ratios reflect phytoplankton community dynamics

Antonia Klatt[1], Cindy De Jonge[2], Daniel B. Nelson[3], Marta Reyes[4], Carsten J. Schubert[5,6], Nathalie Dubois[2,7] & S. Nemiah Ladd[1]*

[1]University of Basel, Department of Environmental Sciences, Organic Geochemistry, Basel, Switzerland (antonia.klatt@unibas.ch)

[2]ETH Zurich, Department of Earth Sciences, Zurich, Switzerland

[3]University of Basel, Department of Environmental Sciences, Botany, Basel, Switzerland

[4]Swiss Federal Institute of Aquatic Science and Technology (Eawag), Department Aquatic Ecology, Dübendorf, Switzerland

[5]Swiss Federal Institute of Aquatic Science and Technology (Eawag), Department Surface Waters – Research and Management, Kastanienbaum, Switzerland

[6]ETH Zurich, Department of Environmental System Science, Zurich, Switzerland

[7]Swiss Federal Institute of Aquatic Science and Technology (Eawag), Department Surface Waters – Research and Management, Dübendorf, Switzerland

Contents:

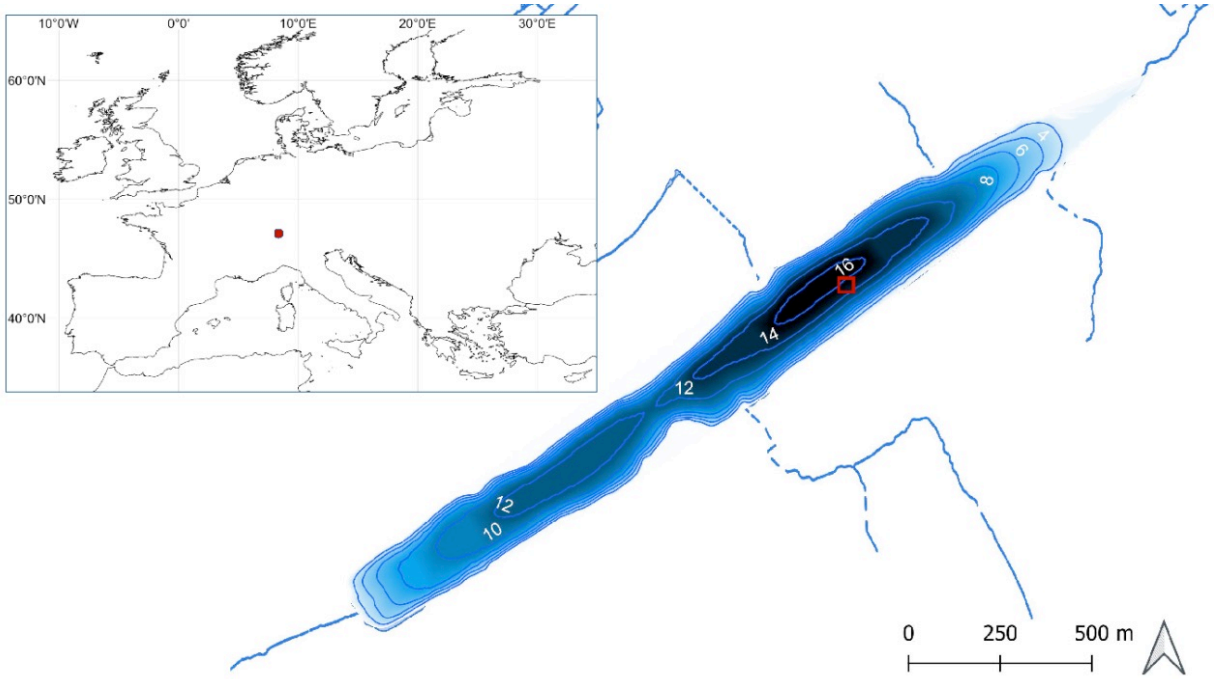

Figure S1: Location (red point) and bathymetry of Rotsee with the sampling area (red box) of biomass samples near the center of the lake. European coastlines were accessed from Natural Earth (https://www.naturalearthdata.com). River connections and bathymetric map of Rotsee were accessed from swissTLM3D and DHM25 (swisstopo.admin.ch) (DHM25 data modified from T. Doda). All maps were produced with QGIS Geographic Information System.

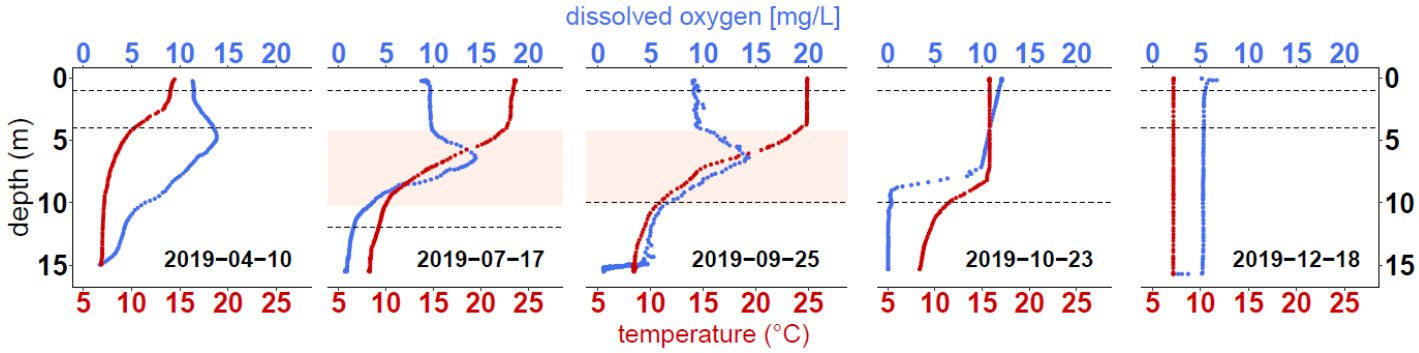

Figure S2: Dissolved oxygen and temperature throughout the water column of Rotsee at different sampling dates representative of different seasons. Only a subset of oxygen and temperature measurements for each date is shown for clarity. The rose-colored areas in summer and early autumn indicate the stable oxycline and thermocline. Dashed lines indicate the respective sampling depths on each sampling date.

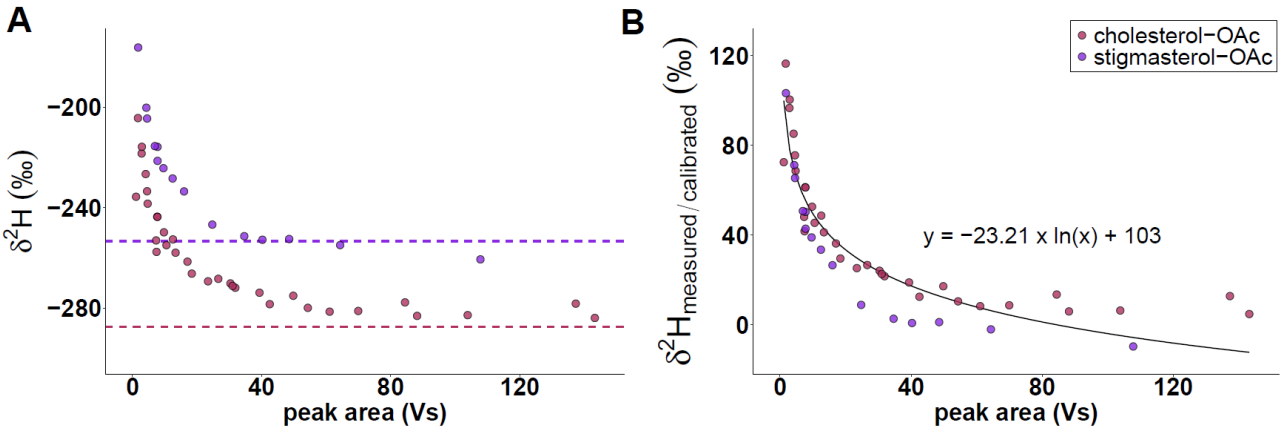

Figure S3: Relationship between measured and calibrated δ^2H values and peak area dimension of cholesterol acetate (cholesterol-OAc) and stigmasterol acetate (stigmasterol-OAc) standards. (A) Relationship between measured δ^2H values and peak area. δ^2H values derived from calibration against reference H_2 gas without further conversion. Dashed lines indicate calibrated δ^2H values based on TC/EA IRMS (cholesterol-OAc) or mean δ^2H values sufficient peak area (stigmasterol-OAc). (B) Relationship between $\delta^2H_{measured/calibrated}$ values and peak area with corresponding formula.

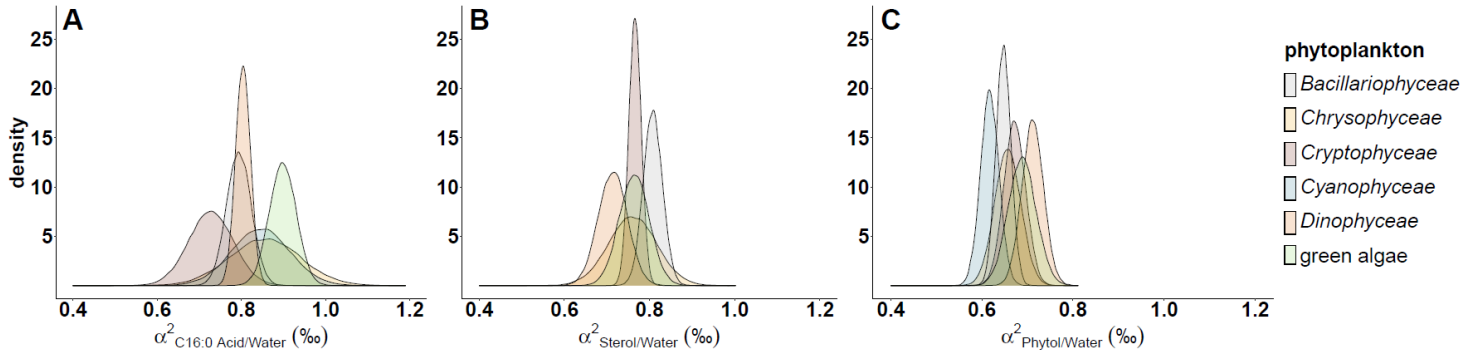

Figure S4: Theoretical distributions of $\alpha^2_{C16:0\ Acid/Water}$ values (A), $\alpha^2_{Sterol/Water}$ values (B), and $\alpha^2_{Phytol/Water}$ values (C) of different phytoplankton groups based on batch cultures from Ladd *et al.* 2024 and Pilecky et al., 2024. Densities were determined by Monte Carlo simulation (n = 50,000) of normal distributions with mean and standard deviation from culturing $\alpha^2_{Lipid/Water}$ values (Ladd *et al.*, 2024; Pilecky *et al.*, 2024). *Chlorophyceae* and *Zygnemopyceae* were summarized to the higher classification 'green algae'. For *Chrysophyceae*, $\alpha^2_{Sterol/Water}$ and $\alpha^2_{Phytol/Water}$ values distributions were simulated based on *Bacillario- and Dinophyceae* due to missing culturing data. No $\alpha^2_{Sterol/Water}$ values were defined for *Cyanophyceae* due to the lack of sterol production.

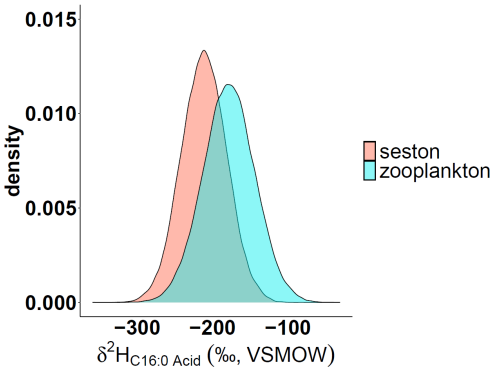

Figure S5: Theoretical distribution of $\delta^2H_{C16:0\ Acid}$ values of seston and zooplankton based on field data from Pilecky *et al.*, 2022. Densities were determined by Monte Carlo simulation (n = 50,000) of normal distributions with mean and standard deviation from field $\delta^2H_{C16:0\ Acid}$ values (Pilecky *et al.*, 2022).

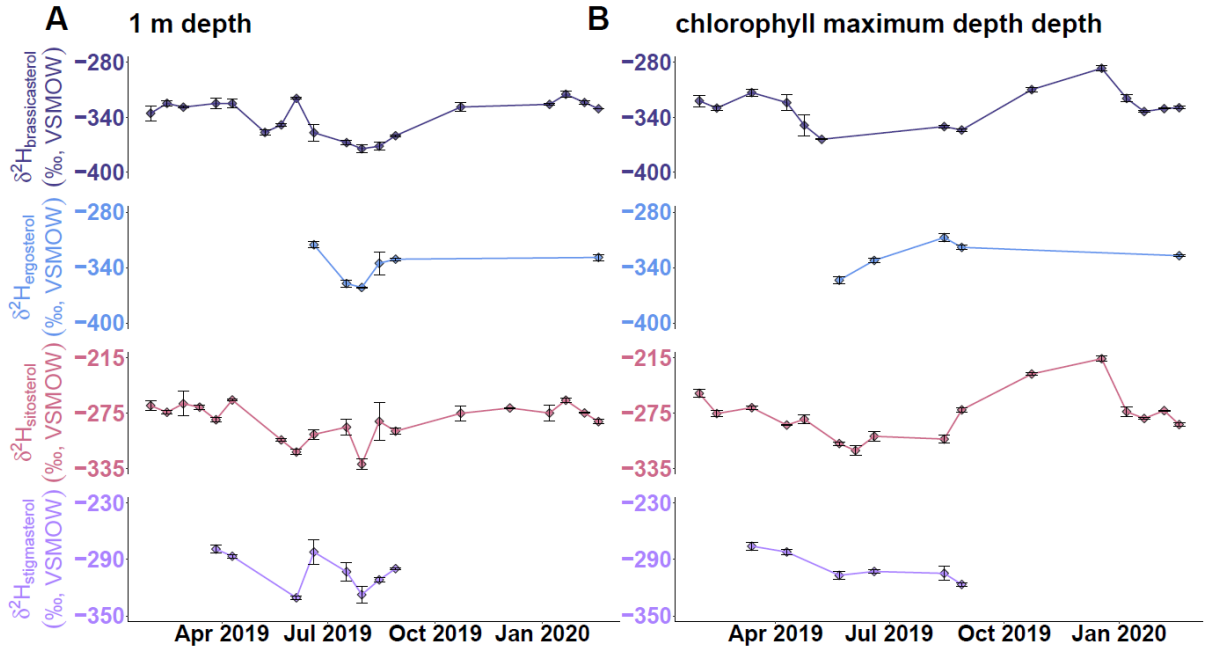

Figure S6: Time series of $\delta^2H_{brassicasterol}$, $\delta^2H_{ergosterol}$, $\delta^2H_{sitosterol}$ and $\delta^2H_{stigmasterol}$ values in Rotsee at 1 m depth (A) and chlorophyll maximum depth (B).

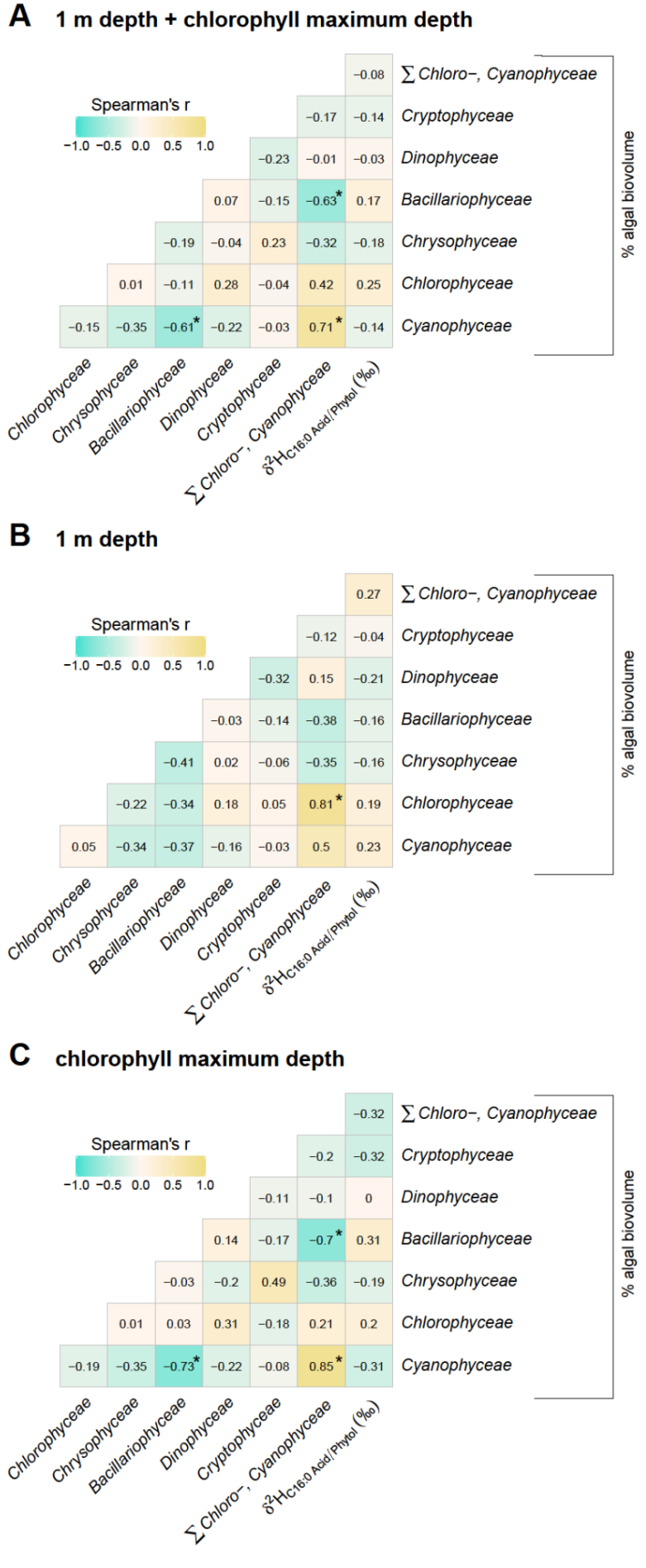

Figure S7: Correlation matrix indicating Spearman's correlations between $\delta^2H_{C16:0\ Acid/Phytol}$ values and the relative biovolume of individual phytoplankton groups in Rotsee combining both sampling depths (A), or at 1 m depth (B) and the chlorophyll maximum depth (C) analyzed separately. r: correlation coefficient. *: $P < 0.05$.

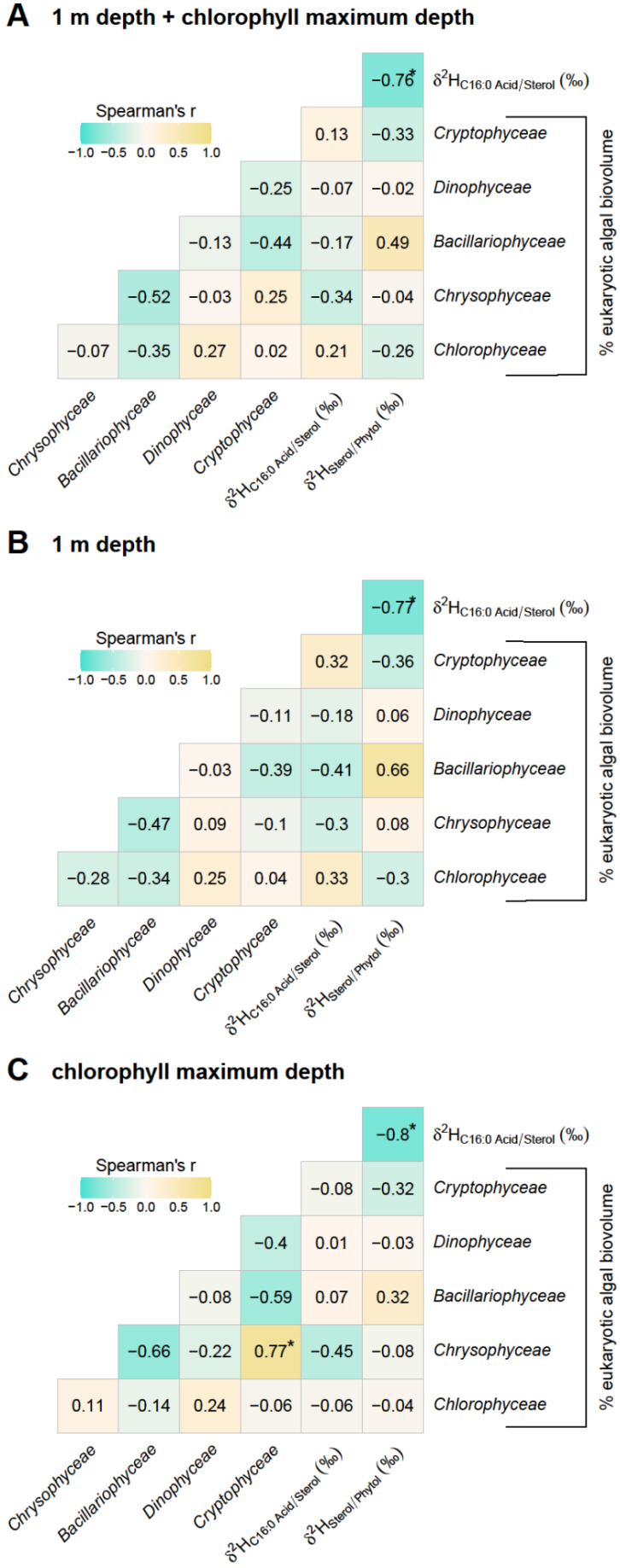

Figure S8: Correlation matrix indicating Spearman's correlations between $\delta^2H_{C16:0\ Acid/Sterol}$ and $\delta^2H_{Sterol/Phytol}$ values and the relative biovolume of individual eukaryotic algal groups in Rotsee combining both sampling depths (A), or at 1 m depth (B) and the chlorophyll maximum depth (C) analyzed separately. Relative contributions from single algal groups to eukaryotic algal biovolume were calculated excluding cyanobacteria. r: correlation coefficient. *: $P < 0.05$.

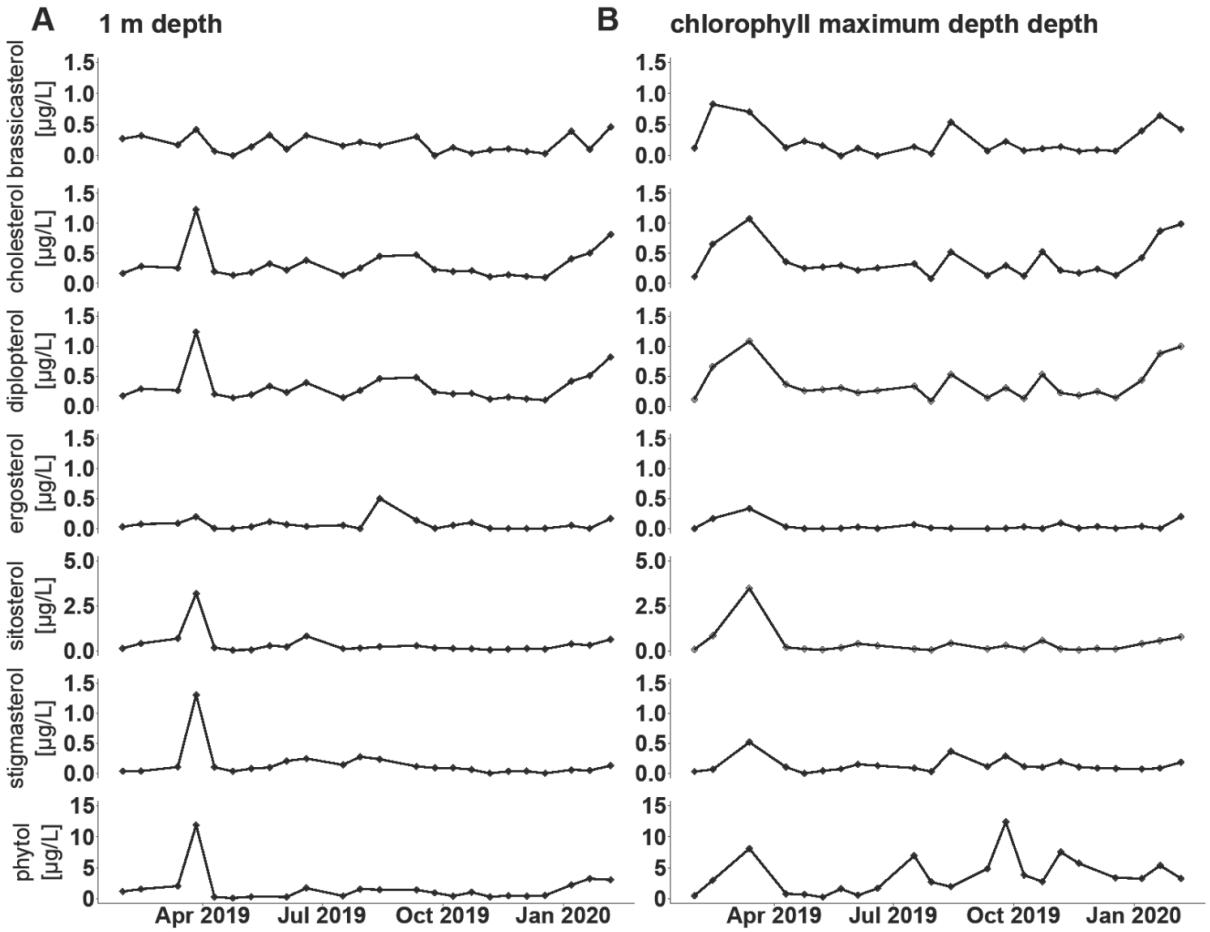

Figure S9: Time series of alcohol concentrations in Rotsee at 1 m depth (A) chlorophyll maximum depth (B). Note the different scaling of y-axes for individual alcohols.

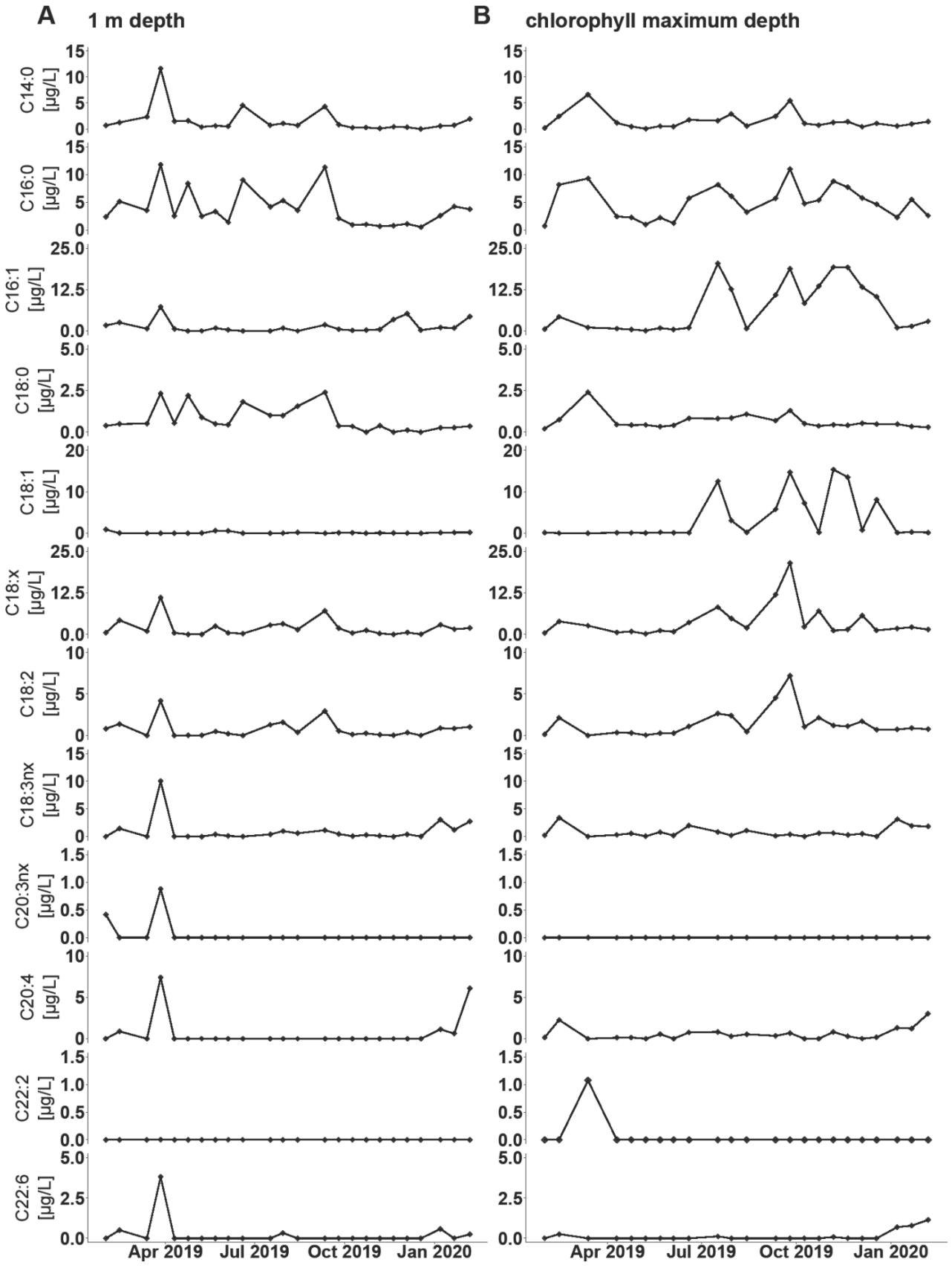

Figure S10: Time series of fatty acid concentrations in Rotsee at 1 m depth (A) and chlorophyll maximum depth (B). Note the different scaling of y-axes for individual fatty acids.

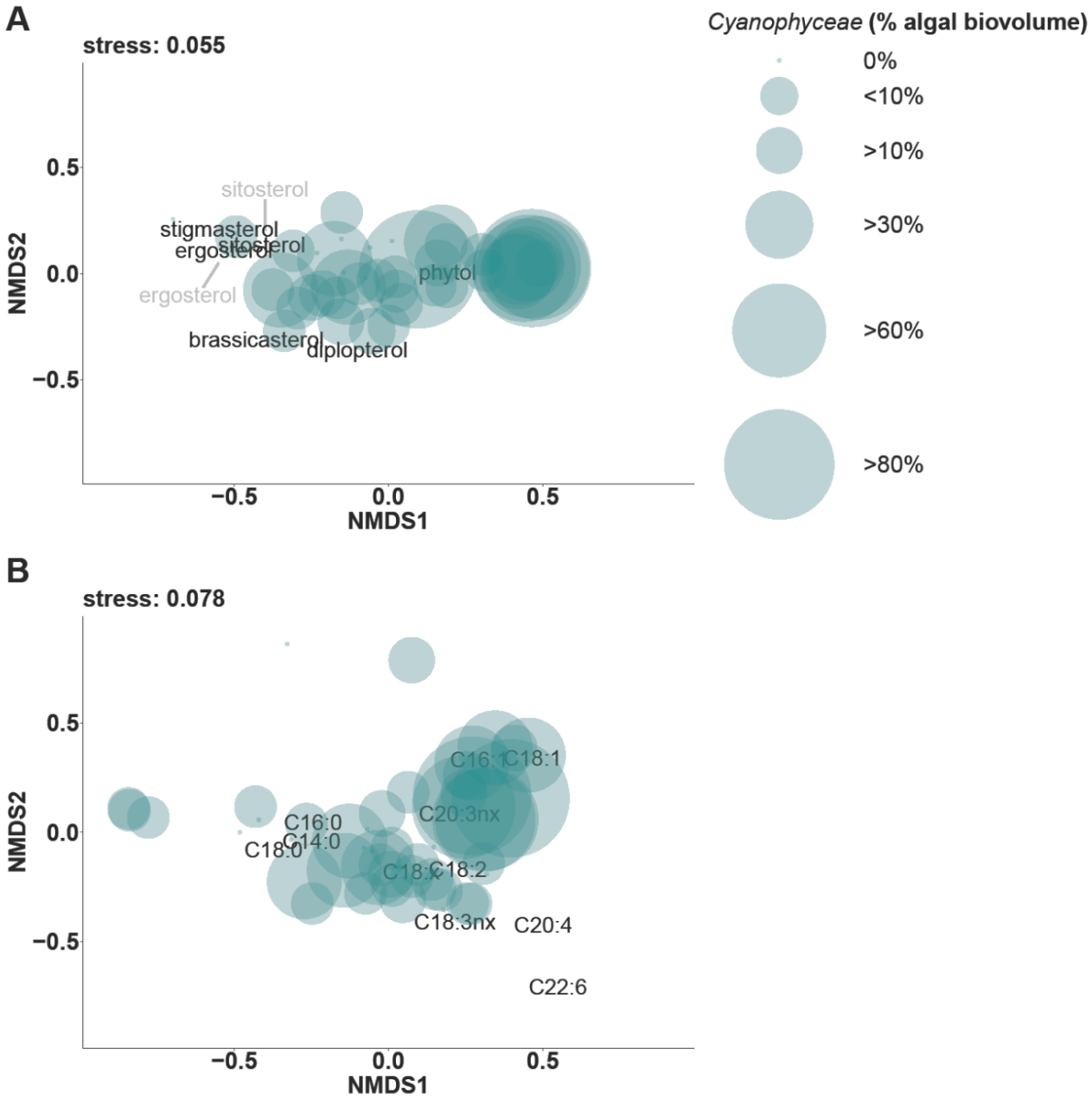

Figure S11: Non-metric-multidimensional scaling (NMDS) of relative alcohol and fatty acid concentrations in the water column of Rotsee. The ordination was set to k=3 dimensions and only the first and second dimensions are shown (NMDS1 vs. NMDS2)). Size scaling of each sample point is based on the relative contribution of cyanobacteria to total phytoplankton biovolume. (A) NMDS of untransformed relative alcohol concentrations. NMDS is based on relative contributions of brassicasterol, diplopterol, ergosterol, phytol, sitosterol and stigmasterol to total alcohol concentrations at single sampling dates, with a final stress of 0.055. (B) NMDS of square root transformed relative fatty acid concentrations. NMDs is based on relative contributions of C14:0, C16:0, C16:1, C18:0, C18:2, C18:3, C18:3nx, C18:x, C20:3nx, C20:4, and C22:6 to total fatty acid concentrations at single sampling dates, with a final stress of 0.078.

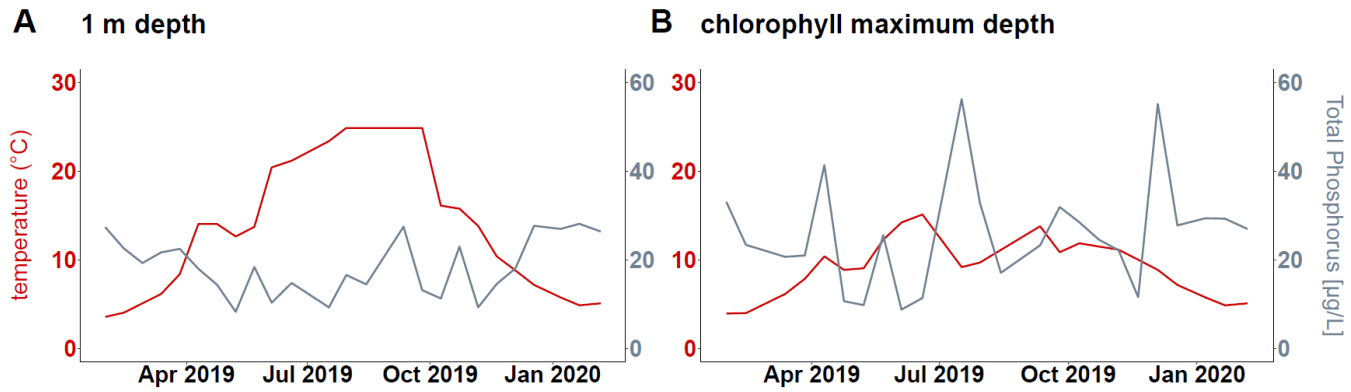

Figure S12: Time series of temperature and total phosphorus concentrations in Rotsee at 1 m depth (A) and the chlorophyll maximum depth (B).

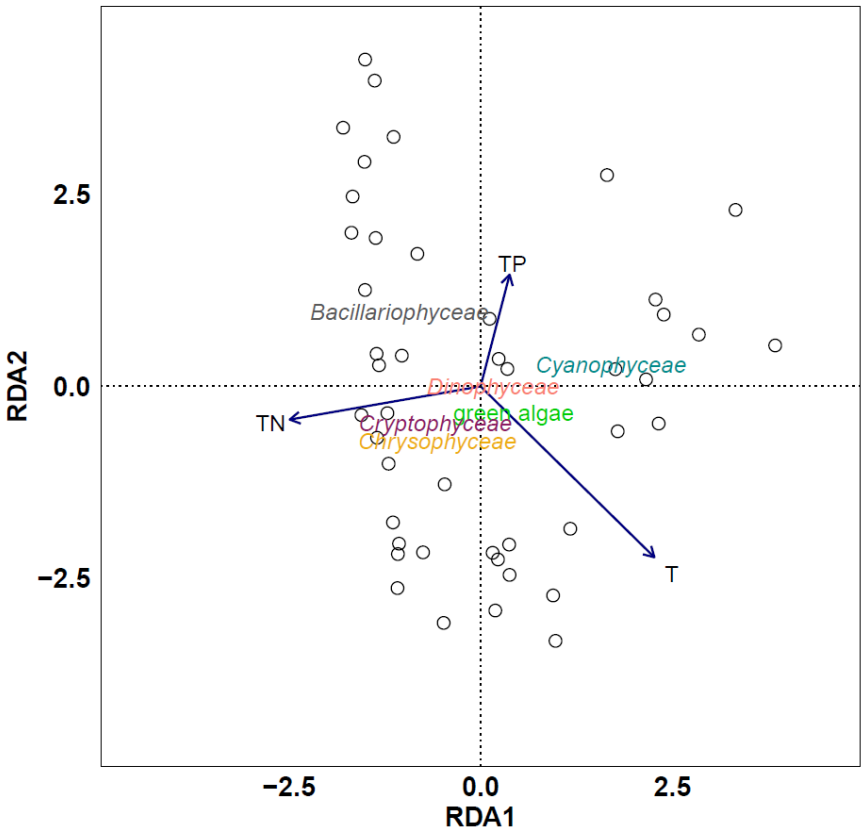

Figure S13: Redundancy analysis (RDA) of relative phytoplankton biovolume and environmental variables (total nitrogen (TN), total phosphorus (TP) and temperature (T)) in Rotsee. Relative biovolume of phytoplankton groups was square root transformed and total phosphorous concentrations were log transformed. TN, TP and T together explained 19.85 % of variance in phytoplankton biovolume ($p = 0.001$). Environmental variables were significantly correlated with each other (TN – TP: $r = 0.5$ $p < 0.001$; TN – T: $r = -0.6$ $p < 0.0001$; TP – T: $r = -0.5$ $p < 0.01$).